CHAPTER 4

RESULTS AND DISCUSSION (PART I):

$LiNbO_3 \cdot SiO_2$ GLASS AND GLASS-CERAMIC SYSTEM

In this chapter, the results are presented for the investigation of (100-*x*)$LiNbO_3 \cdot x SiO_2$ (with *x* = 10, 20, 25, 30, 35, 40, 45, 50 and 60) glasses and glass-ceramics. Appearance, thermal analysis, density, phase analysis, microstructure, optical and electrical properties and their relationships were brought out and discussed. First, the $LiNbO_3$ powder was prepared using the conventional mixed oxide method. Glass former of SiO_2 was then added in various concentrations.

Nine compositions of $LiNbO_3 \cdot SiO_2$ glasses and glass-ceramics were prepared in this study as follows:

(1) $90LiNbO_3 \cdot 10SiO_2$

(2) $80LiNbO_3 \cdot 20SiO_2$

(3) $75LiNbO_3 \cdot 25SiO_2$

(4) $70LiNbO_3 \cdot 30SiO_2$

(5) $65LiNbO_3 \cdot 35SiO_2$

(6) $60LiNbO_3 \cdot 40SiO_2$

(7) $55LiNbO_3 \cdot 45SiO_2$

(8) $50LiNbO_3 \cdot 50SiO_2$

(9) $40LiNbO_3 \cdot 60SiO_2$

4.1 Appearance

4.1.1 Glass samples

Various glass samples with the compositions (100-*x*)$LiNbO_3$ · *x*SiO_2 where *x* = 10, 20, 25, 30, 35, 40, 45, 50 and 60 were prepared using the incorporation method. Glass samples with 20 to 35 mol% SiO_2 were transparent without any visible inclusions and colored lightly yellowish, while products with 10 mol% SiO_2 and 40 mol% SiO_2 exhibited phase separation which both transparent and opaque regions are clearly observed. In addition glass samples with more than 40 mol% SiO_2 were opaque again under the conditions supplied as shown in Fig. 4.1.

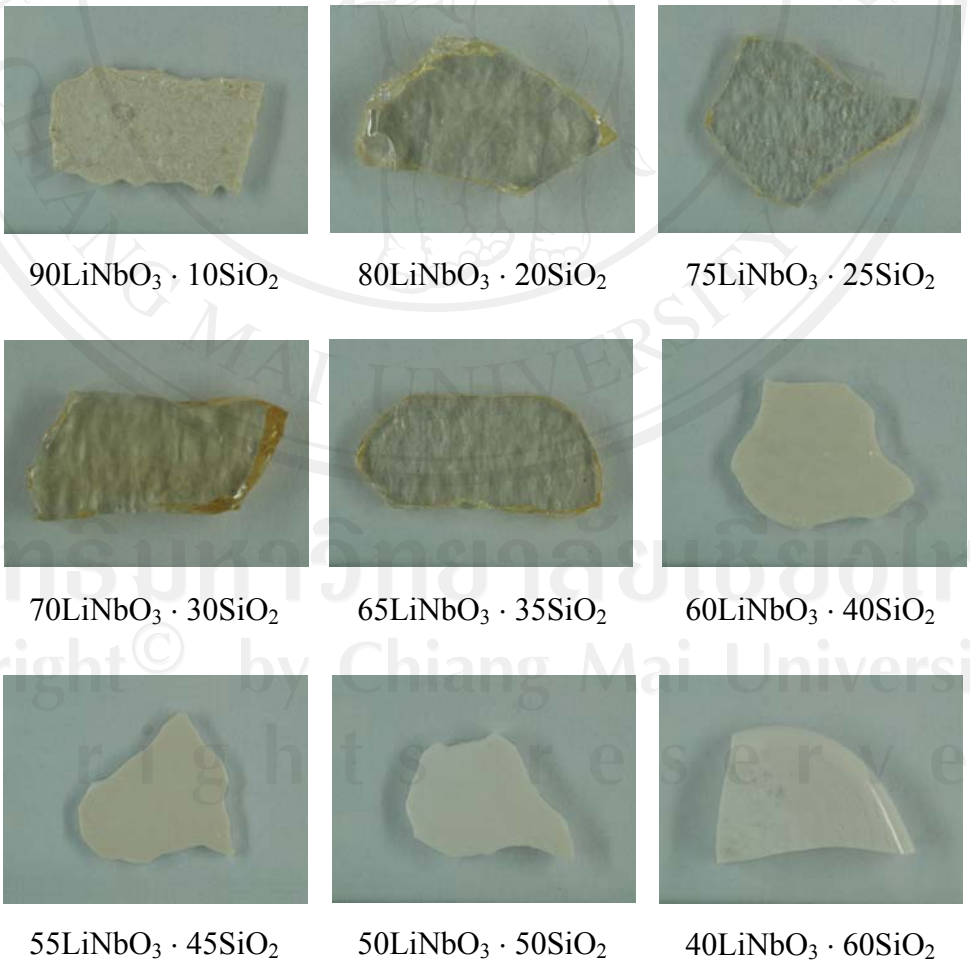

Fig. 4.1 Glass samples with various compositions.

4.1.2 Glass-ceramic samples

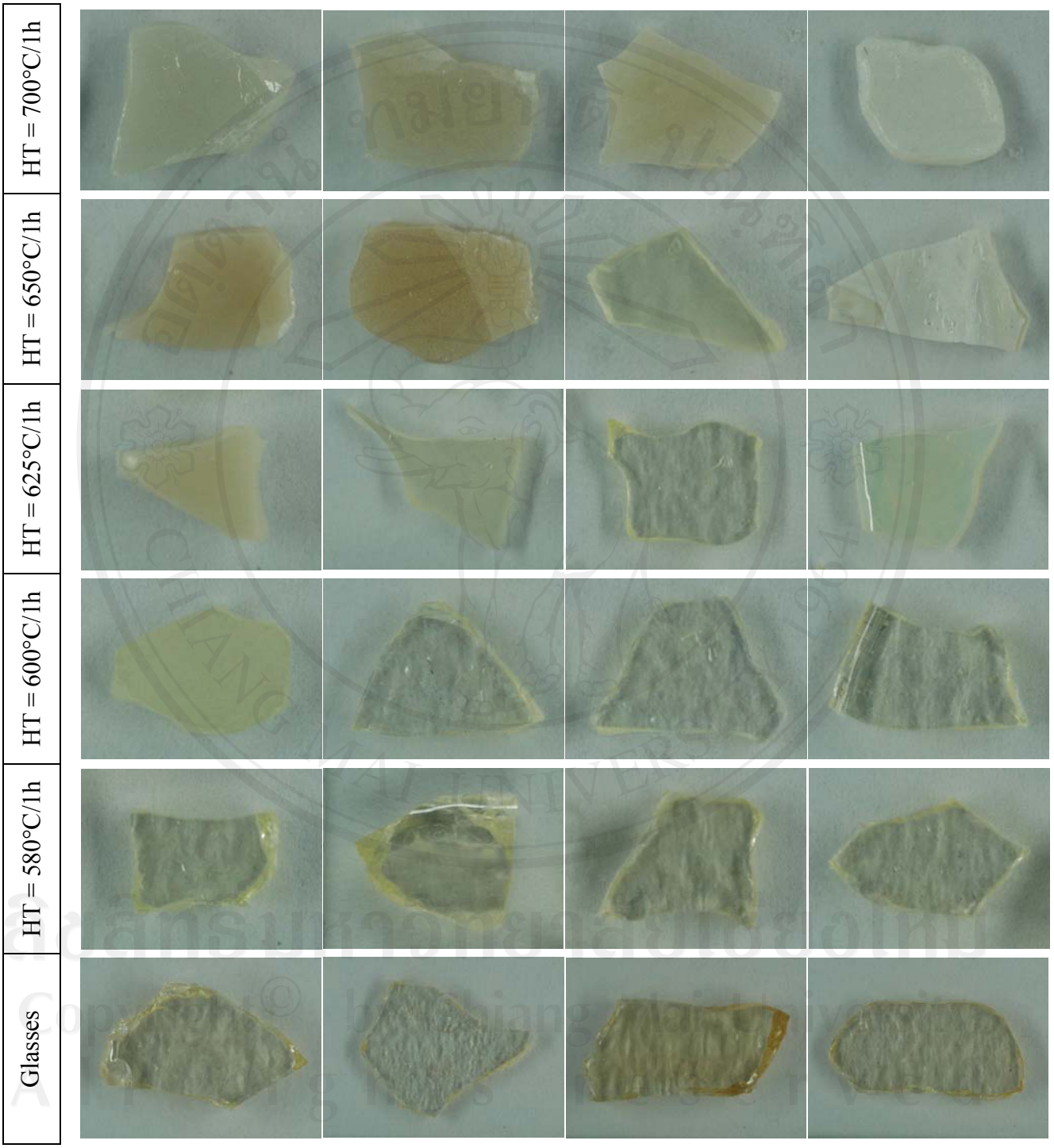

* Note: HT = Heat treatment

Fig. 4.2 Transparency of glasses and glass-ceramics of four compositions.

Transparent glass samples with 20 to 35 mol% SiO_2 were heat-treated at different temperatures (580, 600, 625, 650, 700 and 975 °C) using a heating and cooling rate of 10 K/min for 1 h to convert the glasses to glass-ceramics (Fig. 4.2). However, glass-ceramic samples at 975 °C were not shown in Fig. 4.2; because products started to be opaque, having melted edge, similar to the $65LiNbO_3 \cdot 35SiO_2$ glass-ceramic samples at 700 °C. Besides, high heat treatment temperature had a significant effect on appearance of the samples as the degree of transparency of the samples decreased with increasing heat treatment temperature.

As the $LiNbO_3 \cdot SiO_2$ glasses and glass-ceramics exhibit a fairly broad glass forming range [67]. 20 mol% SiO_2 is large enough to obtain transparent light yellowish and nearly amorphous samples. It is interesting to note that the observed color is similar to that of $LiNbO_3$ single crystals prepared by Czochralski method [87].

4.2 Thermal behavior determination

The use of differential thermal analysis (DTA) has taken advantages to achieve thermal behavior of materials. Glass transition temperature (T_g), crystallization temperature (T_{Cr}) and melting temperature (T_m) of 8 glass samples with the compositions $(100\text{-}x)LiNbO_3 \cdot xSiO_2$ (with x = 20, 25, 30, 35, 40, 45, 50 and 60) were obtained using differential thermal analysis technique (Fig 4.3). The enlarged DTA profiles for each glass compositions were shown in appendix.

The differential thermal analyses of glass samples provide the glass transition temperature as shown in Table 4.1. It can be seen that the trend of glass transition temperature increased with increasing SiO_2 content in the glass (Fig. 4.4). This may

be due to the melting point of $LiNbO_3$ (1257 °C) being lower than that of SiO_2 (1830 °C), so it may reduce both melting temperature and glass transition temperature of the glasses in $LiNbO_3 \cdot SiO_2$ system.

Moreover, the analysis of a differential thermogram also provided crystallization temperature of the glass samples which would be advantaged for producing glass-ceramics by heat-treatment processes. In hypothesis, crystal with single or multiple phases might nucleate in the range of 650 to 700 °C.

The effect of the SiO_2 content on the glass transition temperature is fairly small; within the range of 20 to 35 mol% SiO_2, as it increased less than 20 K. It should be noted that the increase in the crystallization temperature is more pronounced, it increased from 653.7 to 689.5 °C, while increasing the mol% SiO_2 from 20 to 30 as is clearly seen in Fig. 4.4. A further increase leads to a more pronounced phase separation while the crystallization temperature remains approximately constant (690 °C ± 10 K).

At a first glance, it is surprising that the glass transition temperature does not notably depend on the SiO_2 content. However, in the phase separated structure, two phases, a $LiNbO_3$-rich matrix phase and a SiO_2-rich droplet phase are formed as shown in TEM micrographs (Topic 4.5.1), and the amount of these two phases is not normally related to the SiO_2 content. However, without the occurrence of phase separation, the glass transition temperature should linearly increase with the SiO_2 content. In contrast to the $TeO_2 \cdot LiNbO_3$ system, Shankar and Varma [88] reported that the glass transition temperature increased with decreasing TeO_2 content. These

glasses are not phase-separated and the melting point of TeO_2 is 730 °C, i.e. which is much lower than that of SiO_2 (1723 °C).

Table 4.1 Typical DTA curves obtained for the powder of the glass samples corresponding to the compositions.

SiO_2 content (mol%)	**Transition temperatures**			
	T_g (°C)	**T_{Cr1} (°C)**	**T_{Cr2} (°C)**	**T_m (°C)**
20	557	654	969	1172
25	563	680	972	1191
30	571	690	961	1177
35	575	699	973	1158
40	577	678	958	1161
45	567	674	990	1165
50	571	674	976	1162
60	585	675	989	1162

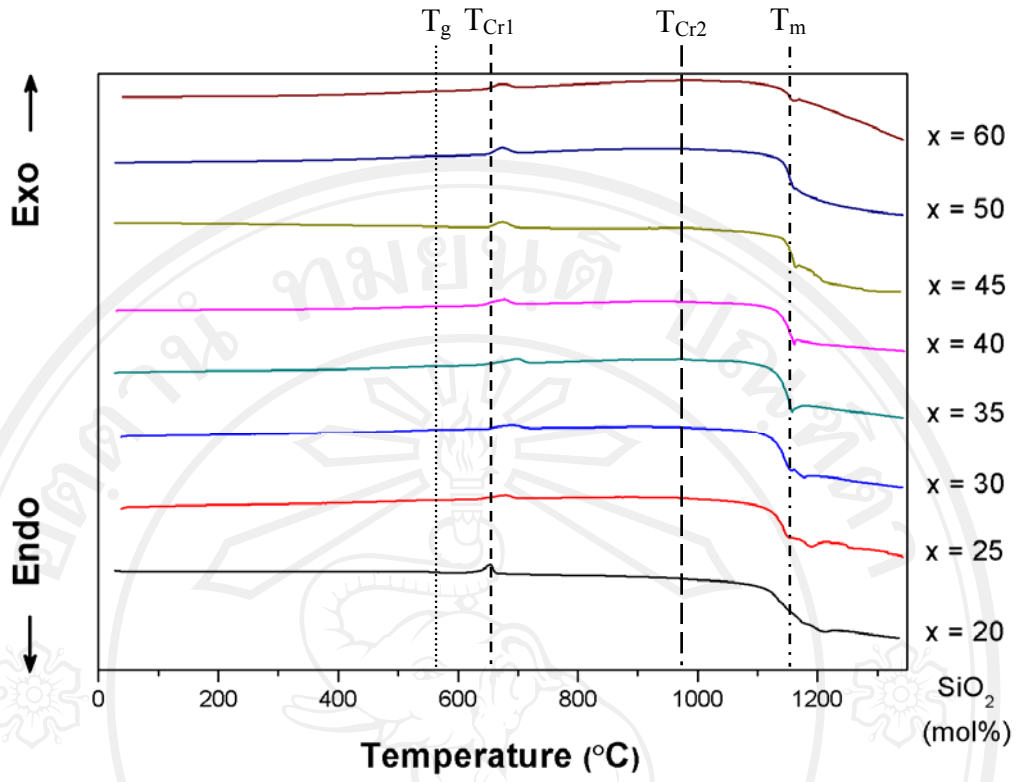

Fig. 4.3 DTA profiles of the glass samples with various compositions.

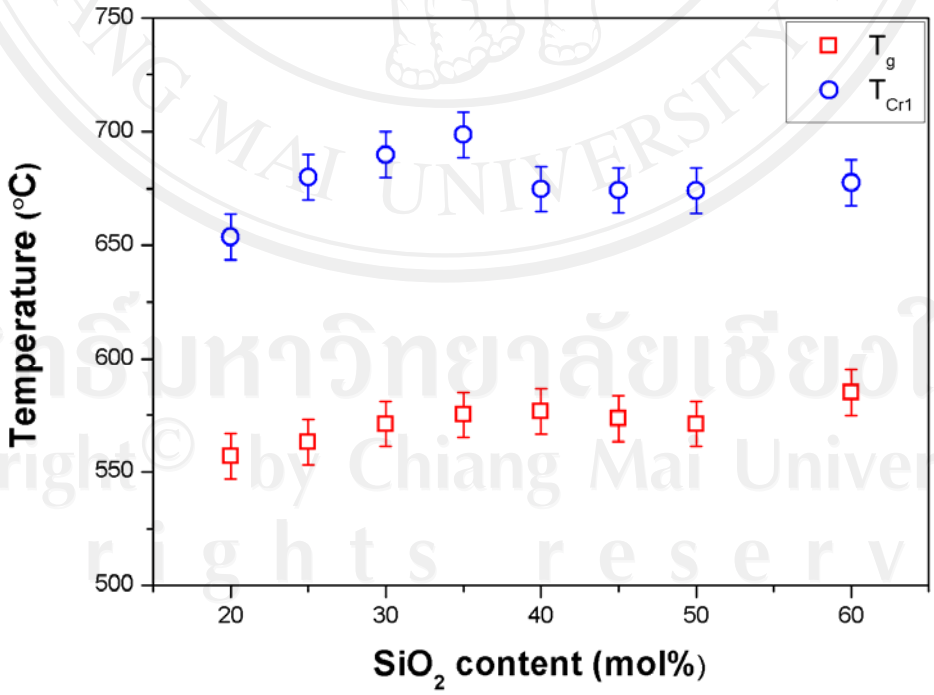

Fig. 4.4 The glass transition temperature (T_g) and the temperature of the first crystallization peak (T_{Cr1}) as a function of mol% SiO_2 (error in the temperatures ± 10 K).

4.3 Densification investigation

The densities of the (100-x)$LiNbO_3$ · $xSiO_2$ (with x = 10, 20, 25, 30, 35, 40, 45, 50 and 60) glasses and glass-ceramics are presented in Table 4.2 and the variation of density with mol% SiO_2 is illustrated in Fig. 4.5. It can be seen that density decreased with increasing mol% SiO_2 or decreasing mol% $LiNbO_3$, because SiO_2 has lower density (ρ = 2.2 g/cm^3) than that of $LiNbO_3$ (ρ = 4.64 g/cm^3).

Table 4.2 Compositional variations of densities measured on the glass and glass-ceramic samples at different heat treatment temperatures.

SiO_2 content (mol%)	**Density (g/cm^3)**			
	Glass samples	**Heat treatment conditions**		
		600 °C / 1 h	**650 °C / 1 h**	**700 °C / 1 h**
10	4.263 ± 0.007	-	-	-
20	3.977 ± 0.002	4.047 ± 0.008	4.200 ± 0.012	4.233 ± 0.007
25	3.899 ± 0.007	3.961 ± 0.002	4.063 ± 0.004	4.102 ± 0.003
30	3.854 ± 0.001	3.910 ± 0.016	3.948 ± 0.002	3.949 ± 0.004
35	3.750 ± 0.009	3.796 ± 0.003	3.855 ± 0.004	3.862 ± 0.007
40	3.664 ± 0.008	-	-	-
45	3.539 ± 0.005	-	-	-
50	3.451 ± 0.002	-	-	-
60	3.224 ± 0.004	-	-	-

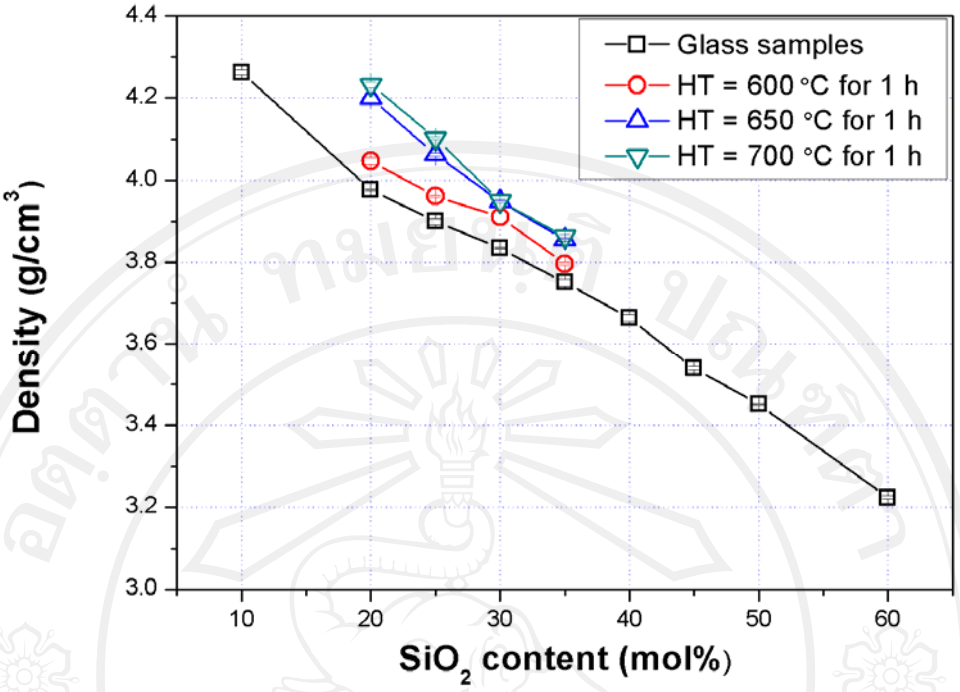

Fig. 4.5 Densities of the glass and glass-ceramic samples at different heat treatment temperatures.

In order to study the crystalline phases formed; these glass samples were heat-treated to their crystallization temperatures as seen in Table 4.1 for 1 h. It can be seen that their densities are higher than that of glass with no crystalline phase. Moreover, glass-ceramics heat-treated at higher temperature have higher density than that of the sample heat-treated at lower temperatures (700 °C > 650 °C > 600 °C > glass samples) (Fig. 4.5), reflecting the importance of heat treatment temperature in controlling the crystallization of the glass-ceramics. Moreover, the heat treatment time is also one of the important parameters of crystallization in glass. As longer the glasses have been heat-treated, higher density of the glass-ceramics can be achieved. (Table 4.3 and Fig. 4.6).

Table 4.3 Compositional variation of densities measured on the glass and glass-ceramic samples at different heating times.

SiO_2 content (mol%)	Density (g/cm^3)			
	Glass samples	Heat treatment conditions		
		600 °C / 1 h	600 °C / 3 h	600 °C / 6 h
20	3.977 ± 0.002	4.047 ± 0.008	4.175 ± 0.013	4.228 ± 0.005
25	3.899 ± 0.007	3.961 ± 0.002	3.998 ± 0.008	4.027 ± 0.007
30	3.854 ± 0.001	3.910 ± 0.016	3.849 ± 0.003	3.878 ± 0.002
35	3.750 ± 0.009	3.796 ± 0.003	3.765 ± 0.002	3.825 ± 0.007

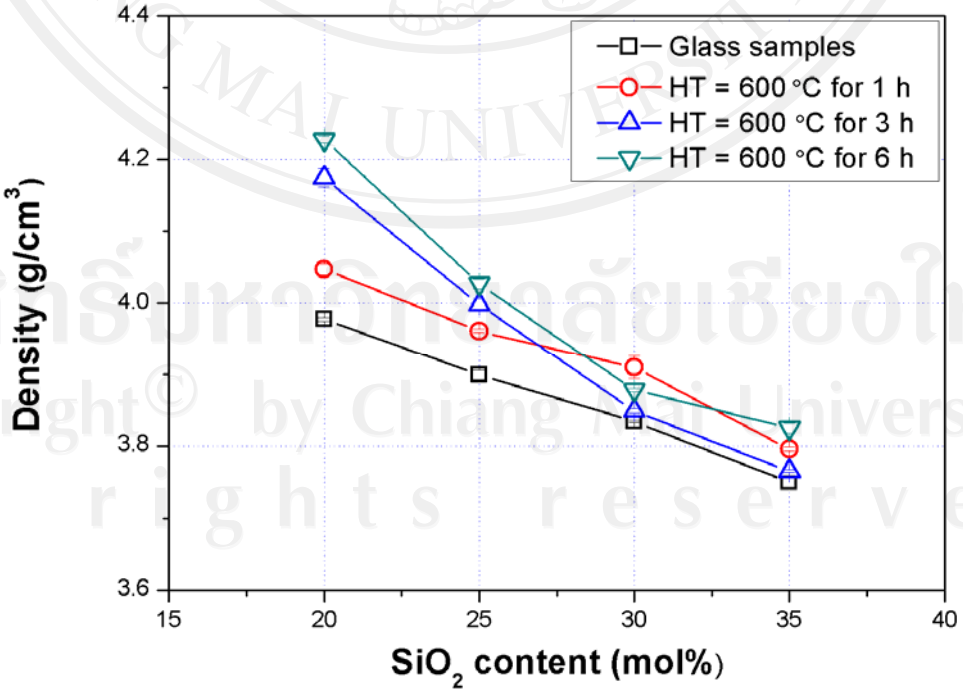

Fig. 4.6 Densities of the glass and glass-ceramic samples at different heating times.

4.4 Structural information

The structural investigation of (100-x)$LiNbO_3$ · $xSiO_2$ (with x = 10, 20, 25, 30, 35, 40, 45, 50 and 60) glasses and glass-ceramics were performed using X-ray diffraction technique to confirm the amorphous nature of the glasses and determine the phase composition of crystallization, nucleation and growth of the glass-ceramics.

The glass sample with 10 mol% SiO_2 shows distinct XRD lines which are all attributable to crystalline $LiNbO_3$ (JCPDS No. 20-0631) and the glass samples with 20 and 25 mol% SiO_2 show lines of marginal intensities also due to $LiNbO_3$; while the glass sample with 60 mol% SiO_2 shows low intensity lines (see 2θ = 22°; red arrow) which were caused by cristobalite (SiO_2; JCPDS file No. 82-0512). The XRD patterns of all other glass samples did not show distinct lines of larger intensity and exhibited an amorphous appearance of the glasses (Fig. 4.7).

From thermal analysis of the glass, the crystallization temperature was used as a condition for producing glass-ceramics from only transparent glasses (20 to 35 mol% SiO_2) by heat treatment control. To produce glass-ceramics, glass plates of each composition were heat-treated at their crystallization temperature with heating and cooling rate of 10 K/min for 1, 3 and 6 h. The results show that crystals might nucleate and grow within the bulk glass. The phase composition of the crystals was confirmed using the X-ray diffraction technique.

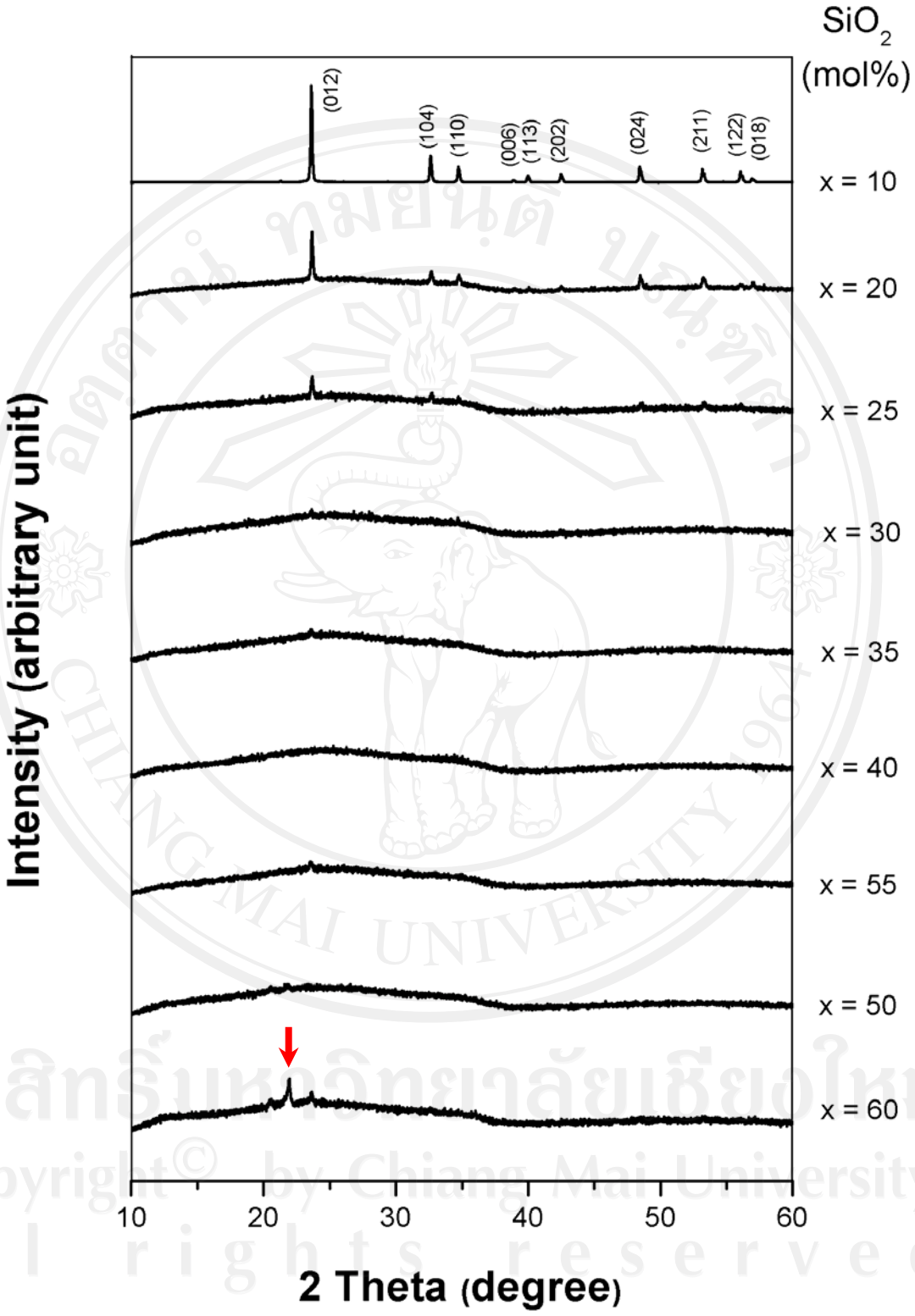

Fig. 4.7 XRD patterns of glass samples with various compositions (red arrow indicates cristobalite phase).

XRD patterns of the glass and glass-ceramic samples with 20 to 35 mol% SiO_2 contents were shown in Fig. 4.8 - Fig. 4.11 for heat treatment temperatures at 600, 650, 700 and 975 °C for 1 h. The XRD lines observed could be attributed to crystalline lithium niobate and indexed as $LiNbO_3$ (JCPDS file No. 20-0631) with lattice parameters a = b = 5.1494 Å and c = 13.862 Å. After heat treatment at 975 °C, additional small intensity lines due to cristobalite phase (JCPDS file No. 82-0512) were observed. The width of the XRD lines decreased with increasing heat treatment temperature. The corresponding full width at half maximum (FWHM) of the observed X-ray peaks as well as the crystallite size calculated using Scherrer equation are shown in Table 4.4. After heat treatment at a temperature of 975 °C, the line broadening is too small to enable the calculation of mean crystallite sizes with acceptable errors. In this case the crystals should be larger than 50 nm.

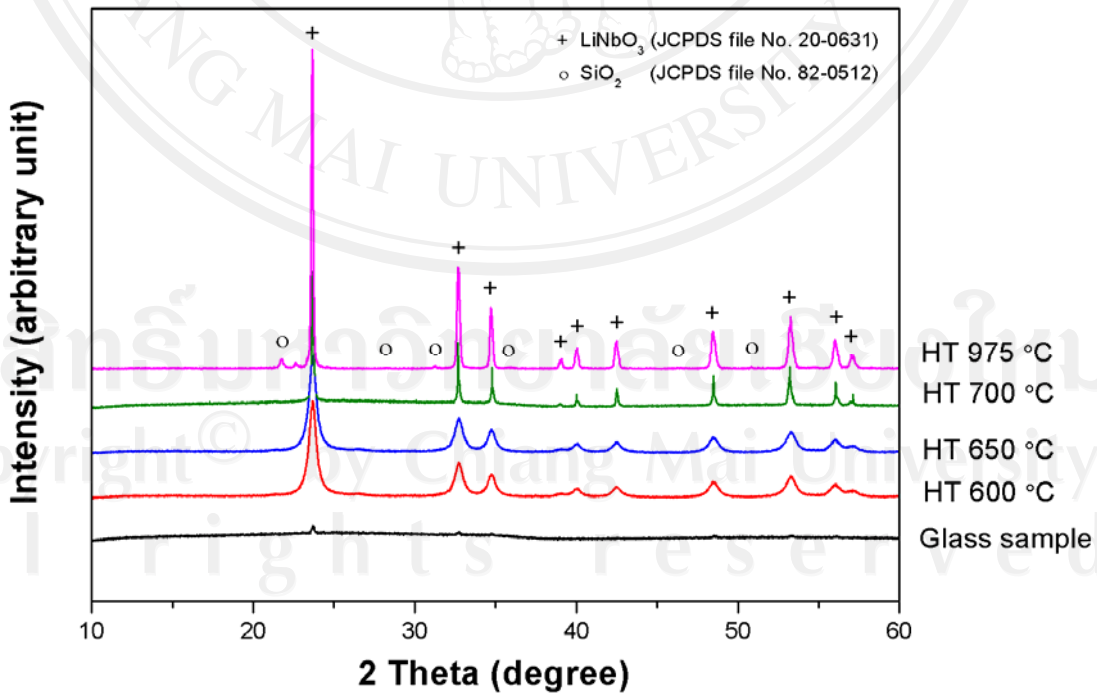

Fig. 4.8 XRD patterns of glass and glass-ceramic samples with 20 mol% SiO_2 at different heat treatment temperatures.

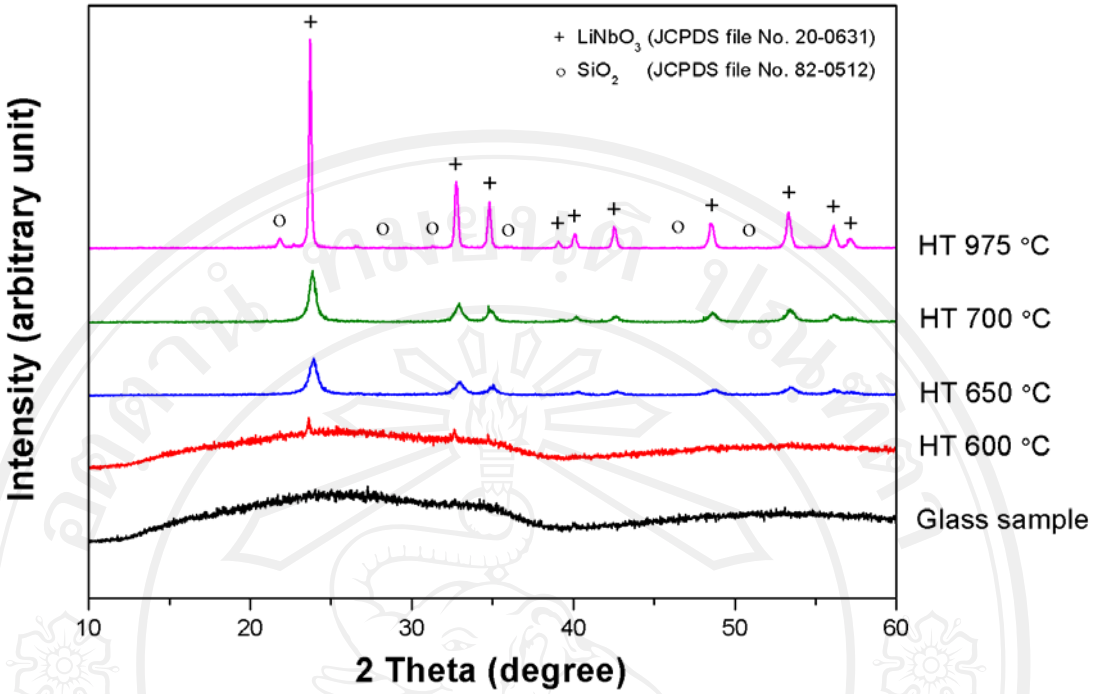

Fig. 4.9 XRD patterns of glass and glass-ceramic samples with 25 mol% SiO_2 at different heat treatment temperatures.

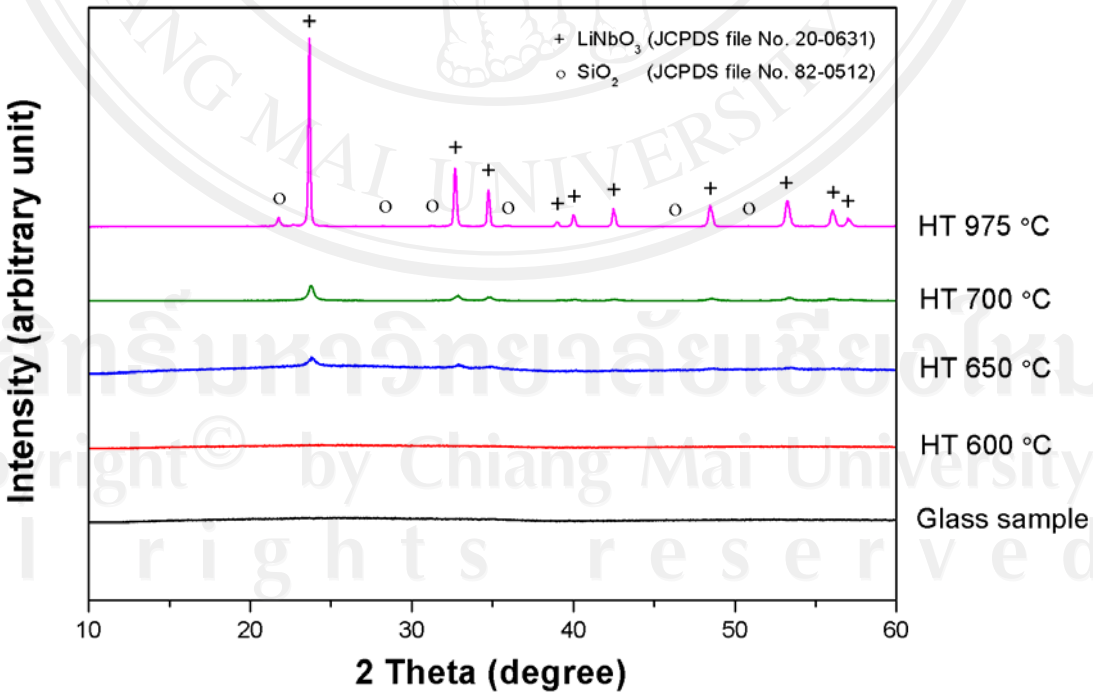

Fig. 4.10 XRD patterns of glass and glass-ceramic samples with 30 mol% SiO_2 at different heat treatment temperatures.

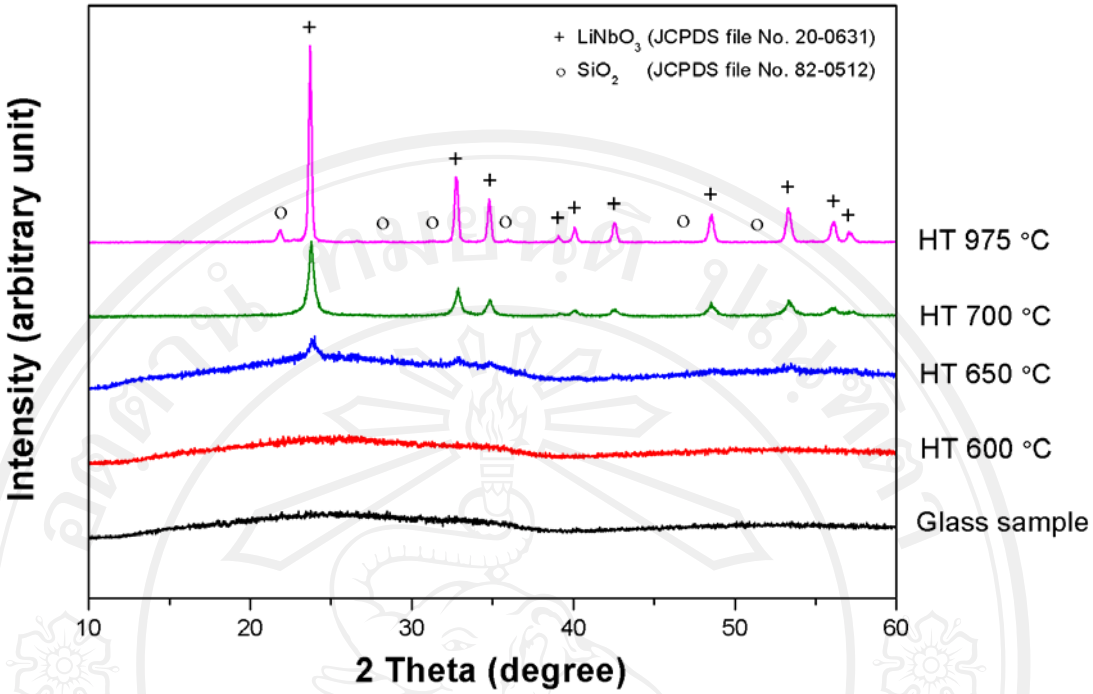

Fig. 4.11 XRD patterns of glass and glass-ceramic samples with 35 mol% SiO_2 at different heat treatment temperatures.

Table 4.4 Mean crystallite sizes (calculated by Scherrer equation) of glass-ceramic samples at 600, 650, 700 and 975 °C for 1 h with 20, 25, 30 and 35 mol% SiO_2.

SiO_2 content (mol%)	Mean crystallite sizes (nm)			
	600 °C	650 °C	700 °C	975 °C
20	15	20	35	42
25	14	23	37	43
30	17	26	42	>50
35	25	47	48	>50

XRD patterns of the glass and glass-ceramic samples with 35 mol % SiO_2 heat-treated at 700 °C (as the first crystallization temperature) for 1, 3 and 6 h are shown in Fig. 4.12 where it can be seen that the crystalline phase in the glass-ceramics heat-treated for 3 and 6 h are the same as that of 1 h which can be indexed as $LiNbO_3$ (JCPDS file No. 20-0631). The width of the XRD lines decreased with increasing periods of times, indicating that the crystallite size also increase with time. Moreover, glass-ceramics heat-treated for a longer time had higher intensities of the $LiNbO_3$ peak than that of the glass-ceramics heat-treated for shorter times (6 h > 3 h > 1 h > glass samples), meaning that not only the size of $LiNbO_3$ increases but also the amount of crystals. The results of the glass and glass-ceramic samples with 20, 25 and 30 mol% SiO_2 are similar.

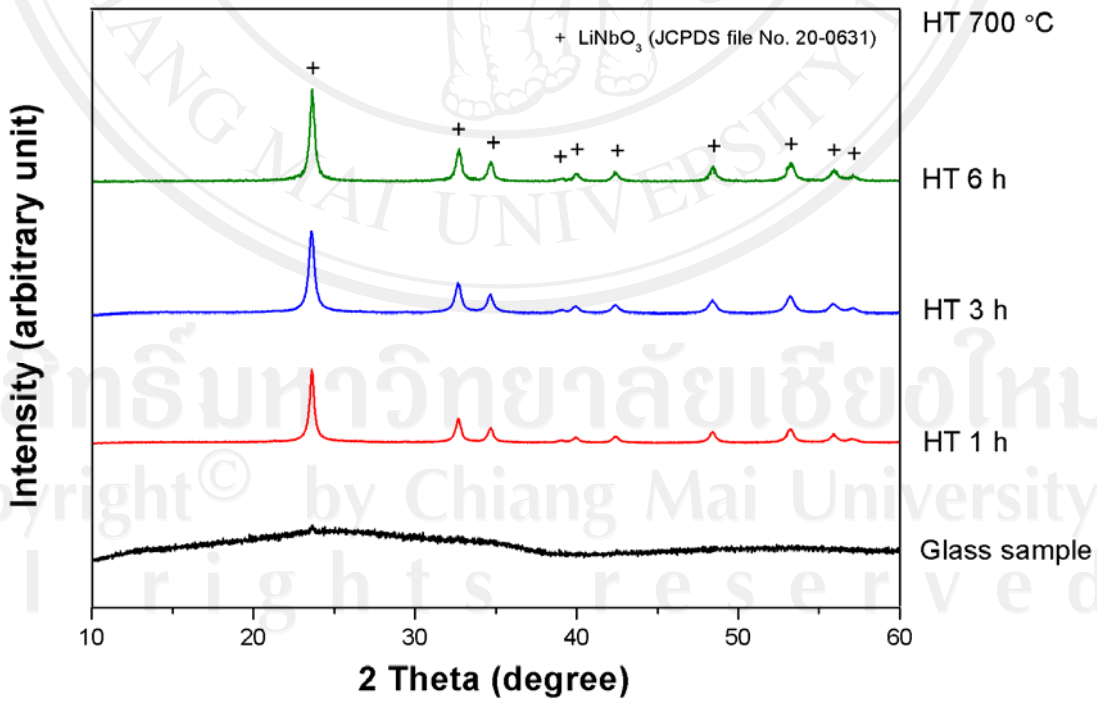

Fig. 4.12 XRD patterns of glass and glass-ceramic samples with 35 mol% SiO_2 at different heating times.

4.5. Microstructure observation

4.5.1 Surface morphology of glass samples

SEM and TEM micrographs of (100-x)$LiNbO_3 \cdot x SiO_2$ (with x = 20, 25, 30, 35, 40 and 50) glass samples show surface morphology of the glass samples. All micrographs possess the same magnification. The glass sample with only 10 mol% SiO_2 contained spontaneous crystallization of $LiNbO_3$. The amount of 20 mol% SiO_2 under the cooling conditions applied, however, was large enough to provide transparent and mainly amorphous samples, which, however, exhibit some heterogeneity with sizes in the range of 30 to 50 nm (Fig. 4.13). The glass sample with 25 mol% SiO_2 is notably more homogeneous. The average size of the heterogeneities is below 30 nm (Fig. 4.14). Then, with increasing SiO_2 content, the size of the structures observed in the TEM micrographs increased again. Todorovic and Radonjic [67] already reported about phase separation in the $Li_2O \cdot Nb_2O_5 \cdot SiO_2 \cdot Al_2O_3$ glass system. In a glass with SiO_2 content of 37.2 and Al_2O_3 content of 5.4 mol%, droplets with diameters in the range of 20 to 50 nm were formed during heat treatment at 610 °C for 10 min. Also these samples were reported to be transparent. In our work, the glass sample with 30 mol% SiO_2 had larger heterogeneities of approximately 150 nm (Fig. 4.15). In the glass sample with 35 mol%, the structures observed exhibited a size of around 250 nm and appeared as elongated droplets (Fig. 4.16). Glass sample with 40 mol% SiO_2 showed light scattering and was opaque. Since its XRD patterns did not show lines of large intensities, the light scattering is caused by phase separation. As shown in the TEM micrographs (Fig. 4.17), droplets with a size of 350 nm were observed. In principle, all glass samples which exhibited phase separation with structures larger than 100 nm should be opaque [89]. In our

work, the glass sample with 50 mol% SiO_2, had sizes of the heterogeneous structures of around 450 nm (Fig. 4.18). In the case of the glass samples with 40 and 50 mol% SiO_2, the droplet shape of the heterogeneities also gave evidence for phase separation. During the course of the phase separation process, supposedly $LiNbO_3$- and SiO_2-rich phases were formed.

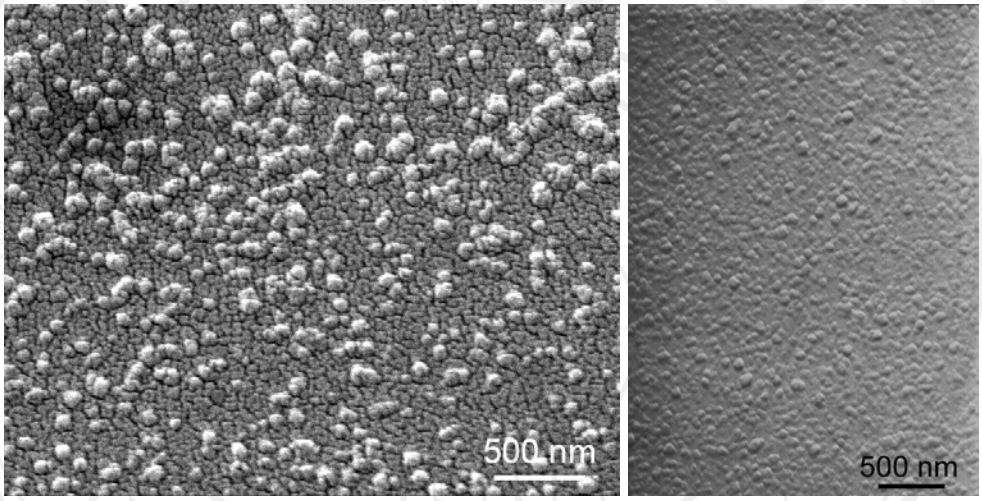

Fig. 4.13 SEM and TEM micrographs of the glass sample with 20 mol% SiO_2.

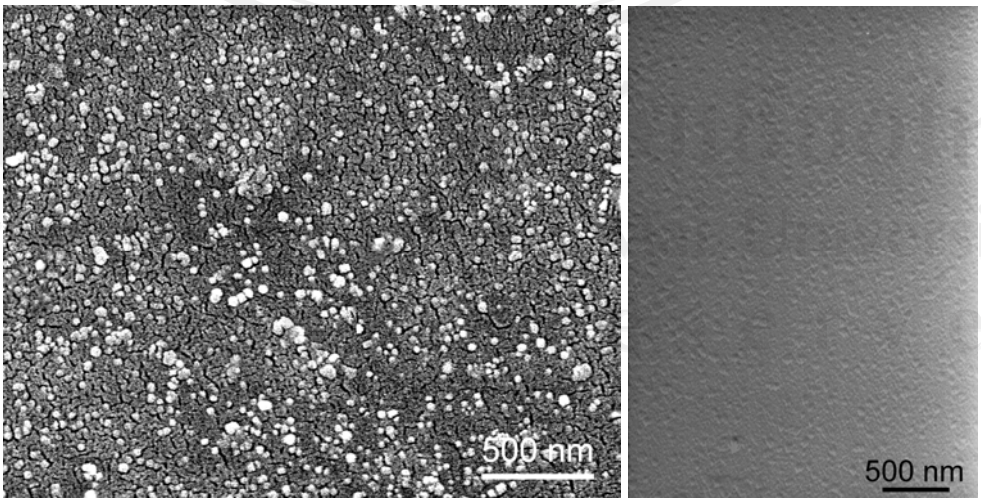

Fig. 4.14 SEM and TEM micrographs of the glass sample with 25 mol% SiO_2.

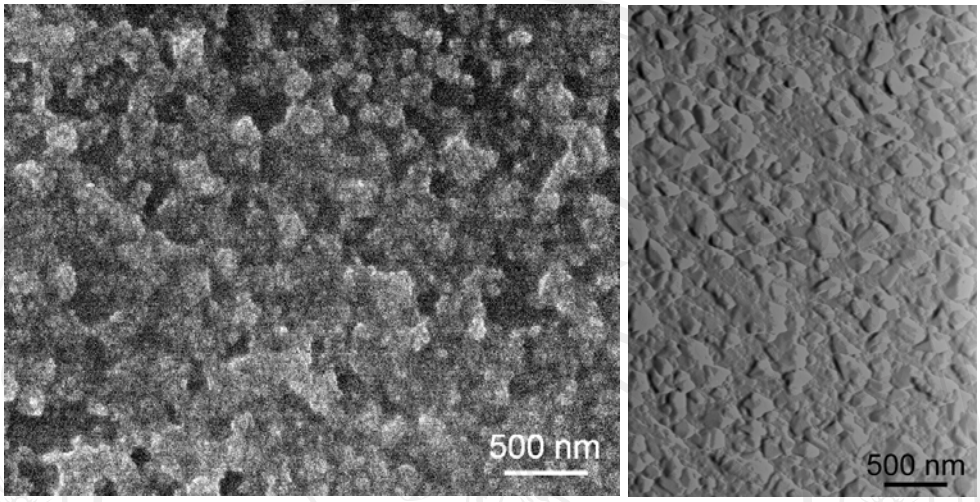

Fig. 4.15 SEM and TEM micrographs of the glass sample with 30 mol% SiO_2.

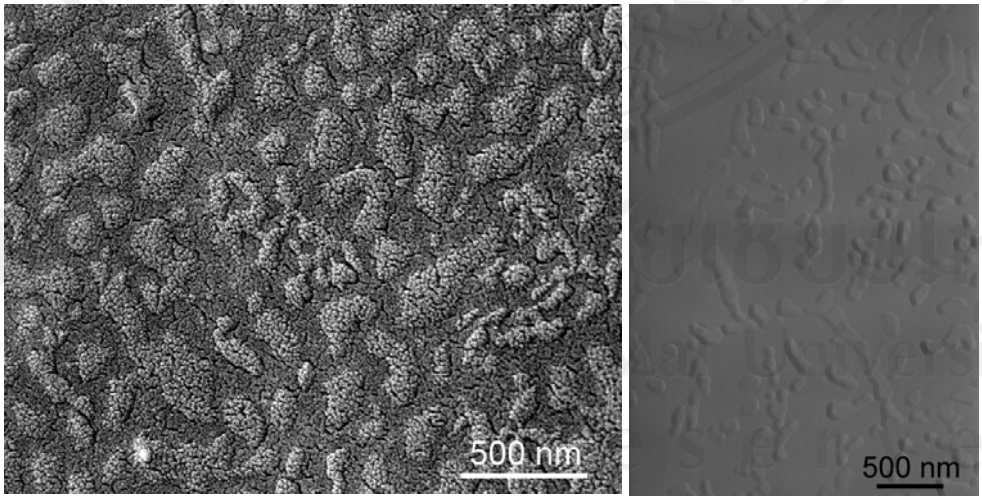

Fig. 4.16 SEM and TEM micrographs of the glass sample with 35 mol% SiO_2.

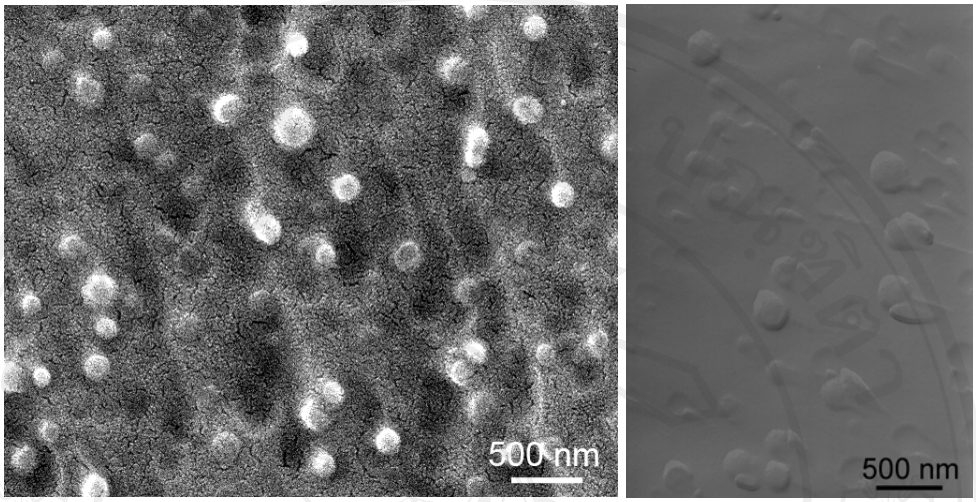

Fig. 4.17 SEM and TEM micrographs of the glass sample with 40 mol% SiO_2.

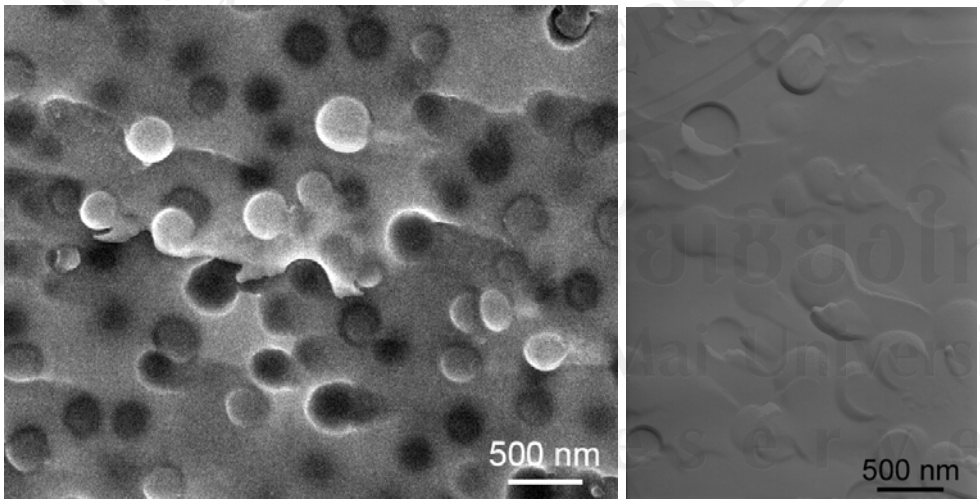

Fig. 4.18 SEM and TEM micrographs of the glass sample with 50 mol% SiO_2.

In the SEM micrographs (BSE detector) of glass-ceramic samples (Fig. 4.19); spherical structures as well as a matrix phase of light appearance were observed. The size of the spherical structures was approximately the same as that of the droplet phase. The dark appearance phase is the SiO_2-rich phase because this phase possesses the smaller mean atomic weight in comparison to the $LiNbO_3$-rich phase. Then, the droplet phase shown in TEM micrographs (Fig. 4.17 - Fig. 4.18) should also be the SiO_2-rich phase. During heat treatment process, the matrix phase crystallizes and forms lithium niobate.

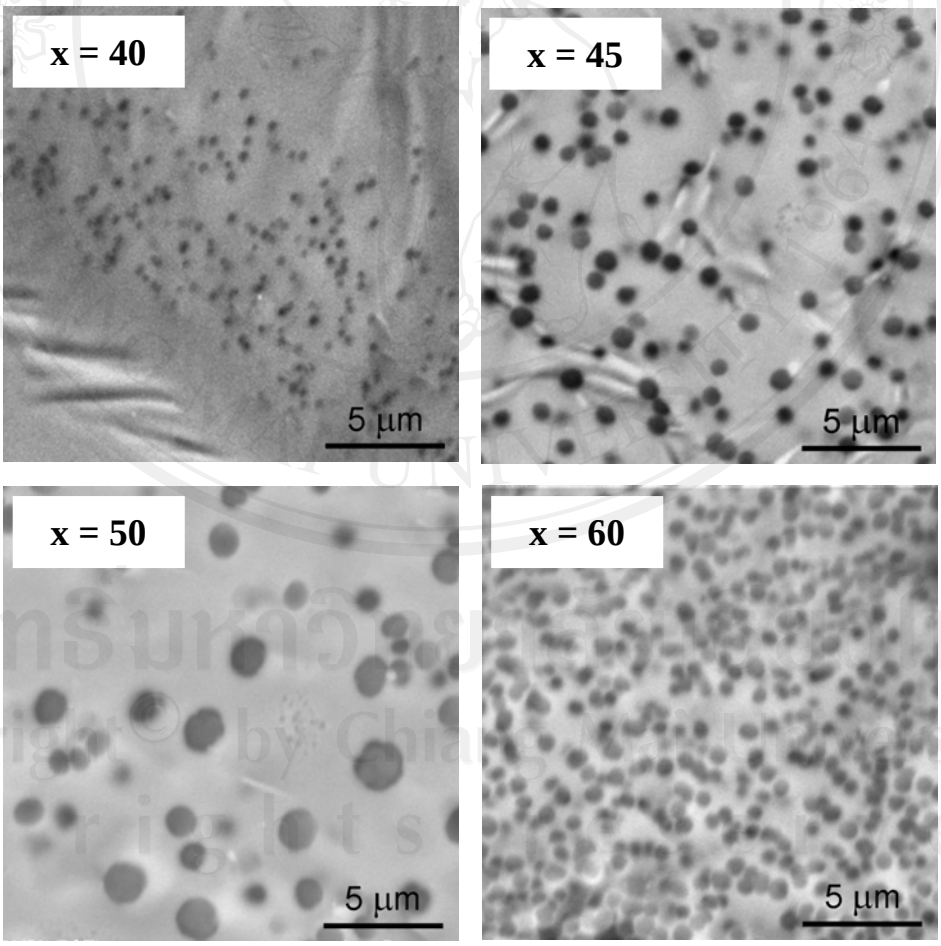

Fig. 4.19 SEM micrographs (BSE detector) of heat-treated samples at 700 °C for 1 h with 40, 45, 50 and 60 mol% SiO_2.

4.5.2 Cross-sectional morphology of glass and glass-ceramic samples

SEM micrographs of cross-sectional morphology of (100-*x*)$LiNbO_3$ · *x*SiO_2 (with *x* = 20, 25, 30 and 35) glasses and glass-ceramics heat-treated at 600, 650, 700 and 975 °C for 1 h were illustrated in Fig. 4.20 - 4.23. All micrographs were taken at the same magnification.

The glass sample with 20 mol% SiO_2 (Fig. 4.20; quenched sample) has crystals with sizes of around 50 nm. According to the XRD patterns, it is the $LiNbO_3$ phase. The glass-ceramic samples heat-treated at 600 and 650 °C contain crystals with sizes from 100 to 150 nm, but at 650 °C the amounts of crystals are much larger. For the glass-ceramic sample heat-treated at 700 °C, the average crystallite size is around 250 nm and disperses well in the glass matrix. Finally, the glass-ceramic sample heat-treated at 975 °C contains $LiNbO_3$ (light phase) as well as cristobalite (dark phase) crystals with sizes in the range of 300 to 500 nm (Fig. 4.20). It can be assumed that the heat treatment temperature plays significant role in controlling the microstructure, crystallite sizes and crystal quantity of the glass-ceramics [90] as raw data was showed in appendix.

Phase separation was observed in all glass samples with 25, 30 and 35 mol% SiO_2, however, according to the XRD patterns, they are amorphous. Moreover, similar results were observed in the glass-ceramic samples containing 25 - 35 mol% SiO_2 as described for the 20 mol% SiO_2 sample, as seen in Fig. 4.21 - 4.23. However, the sizes and quantity are different depending on SiO_2 content and heat treatment temperature. The observed SEM micrographs can be related to the appearance of the samples (Section 4.1), involving their transparency or opacity. For visible light (400 to 800 nm in wavelength), samples possessing crystals larger than 200 nm should

show light scattering and hence the respective samples should be opaque [91, 92]. In our work, transparent samples should have crystals less than 200 nm. In addition, the effect of temperature on the mean size of the crystals was surprisingly small: for example in the sample with 30 mol% SiO_2: the size are 50 nm after heat treatment at 600 °C, giving rise to all transparent glass-ceramics for this composition. During crystallization of $LiNbO_3$, the residual glassy phase is enriched in SiO_2, therefore their viscosities should increase during the course of the crystallization. In analogy to previous reports on the crystallization of CaF_2 [93] from silicate glasses, this should lead to a diffusion barrier around the crystals which hinders crystal growth as well as Ostwald ripening.

During heat treatment of the glass samples, crystallization of lithium niobate occurs. Other phases, such as $LiNb_3O_8$ were not observed [94, 88]. Kim *et al* [8] studied glasses in the $LiNbO_3 \cdot SiO_2$ system; however, they quenched the melts by using a twin roller technique. They reported the occurrence of two exothermic peaks in the DTA profiles which are attributed to crystallization of $LiNbO_3$ and $Li_6Si_2O_7$, respectively.

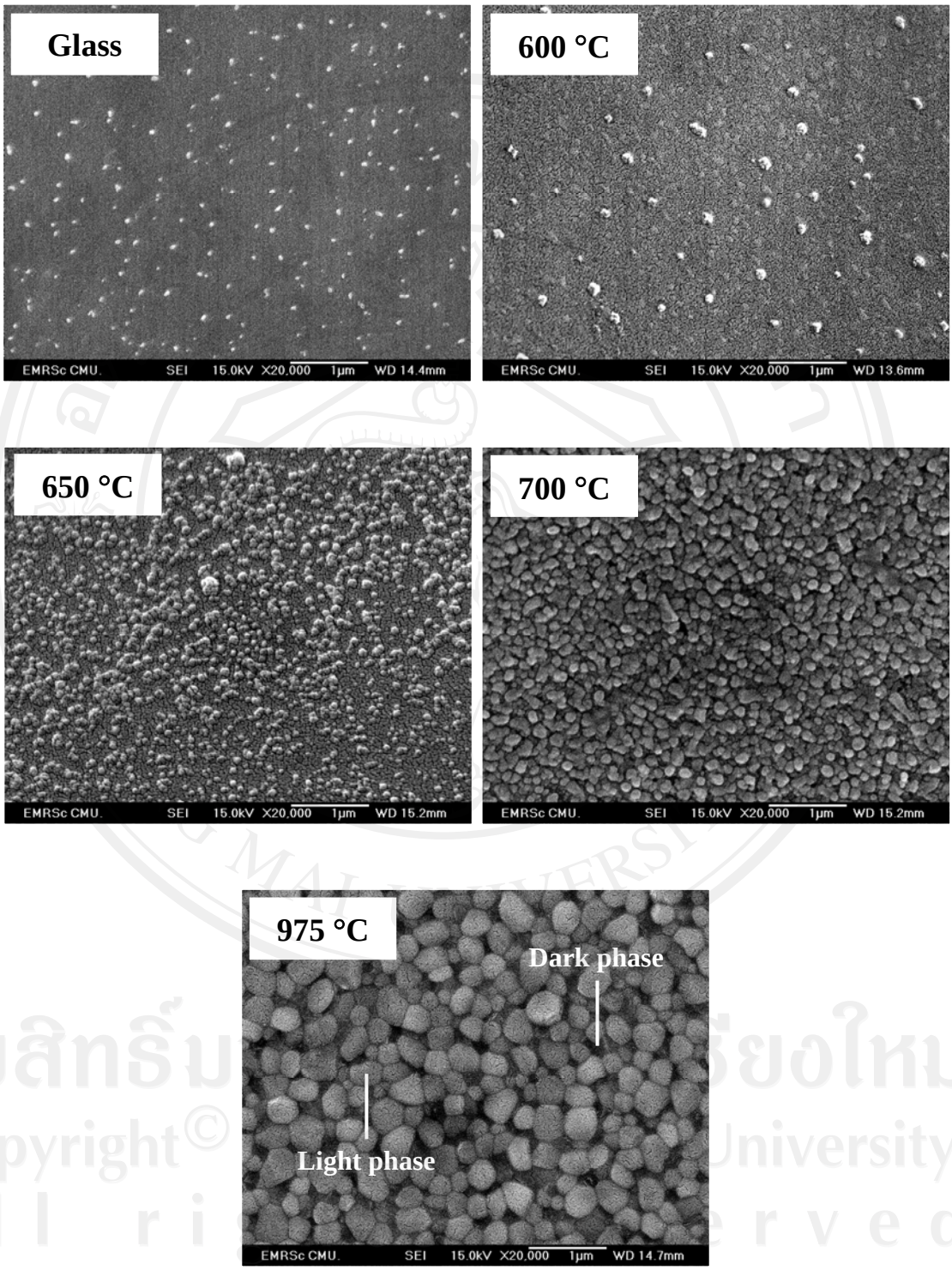

Fig. 4.20 SEM micrographs of the glass and glass-ceramic samples with 20 mol% SiO_2.

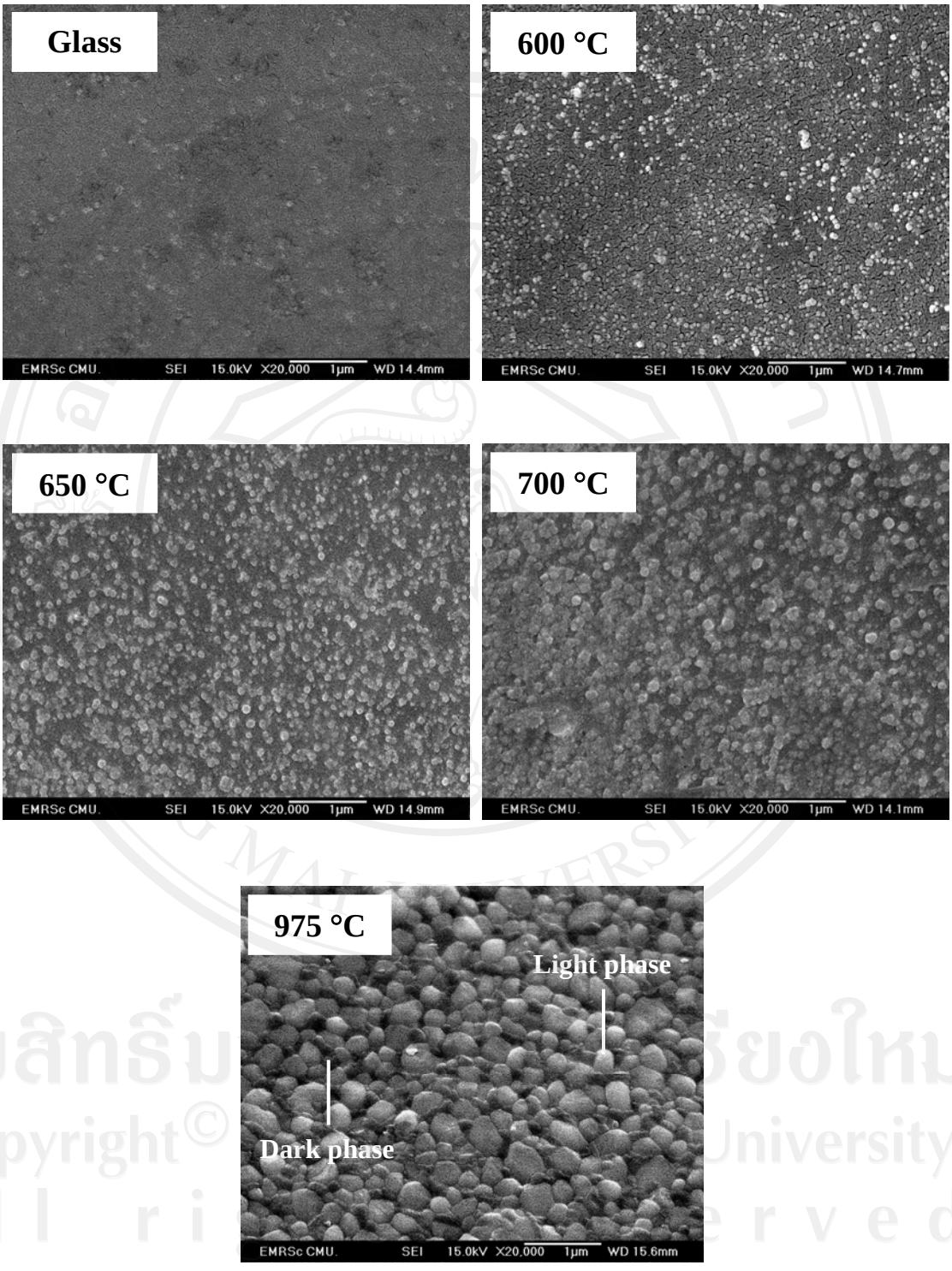

Fig. 4.21 SEM micrographs of the glass and glass-ceramic samples with 25 mol% SiO_2.

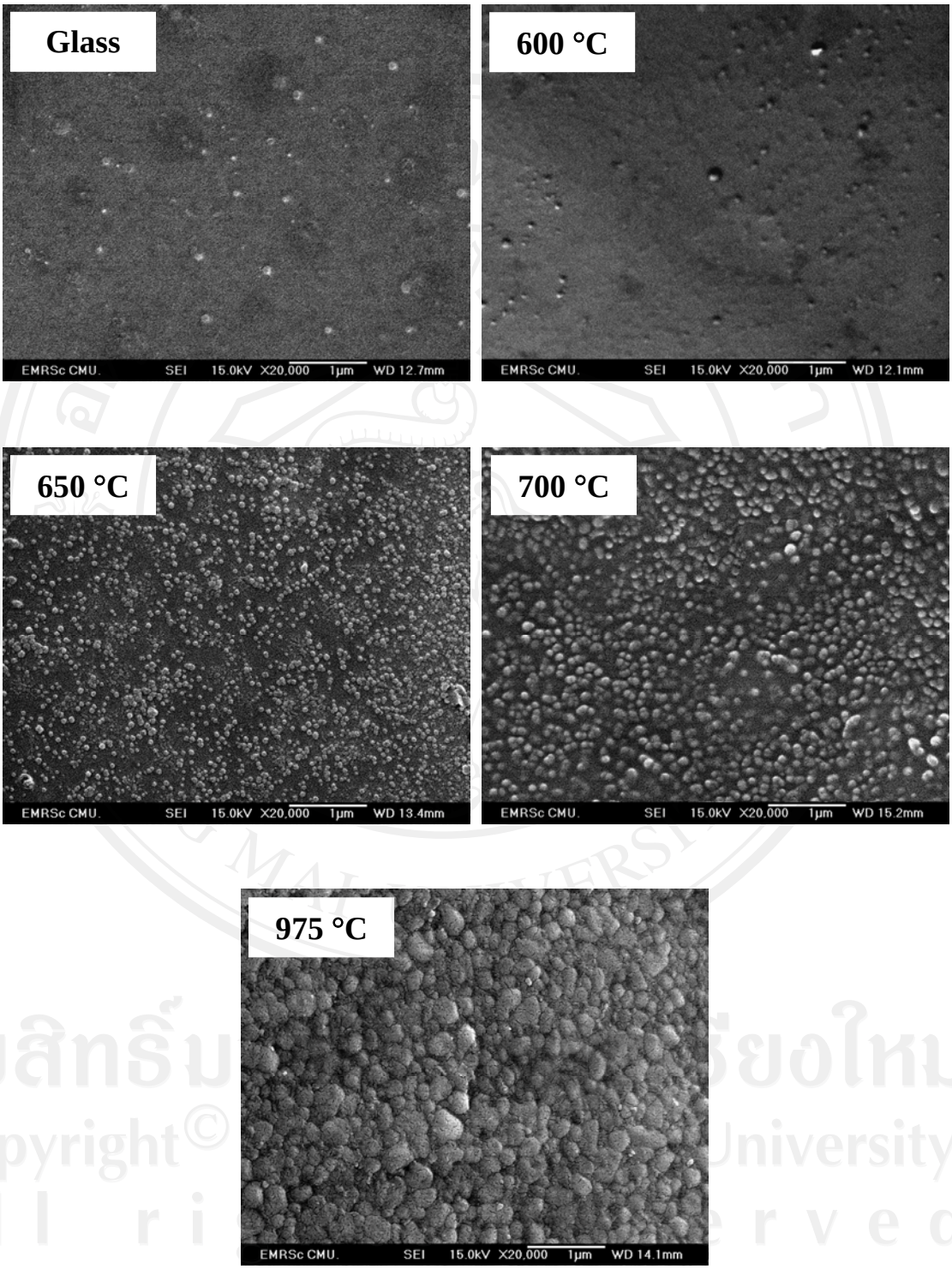

Fig. 4.22 SEM micrographs of the glass and glass-ceramic samples with 30 mol% SiO_2.

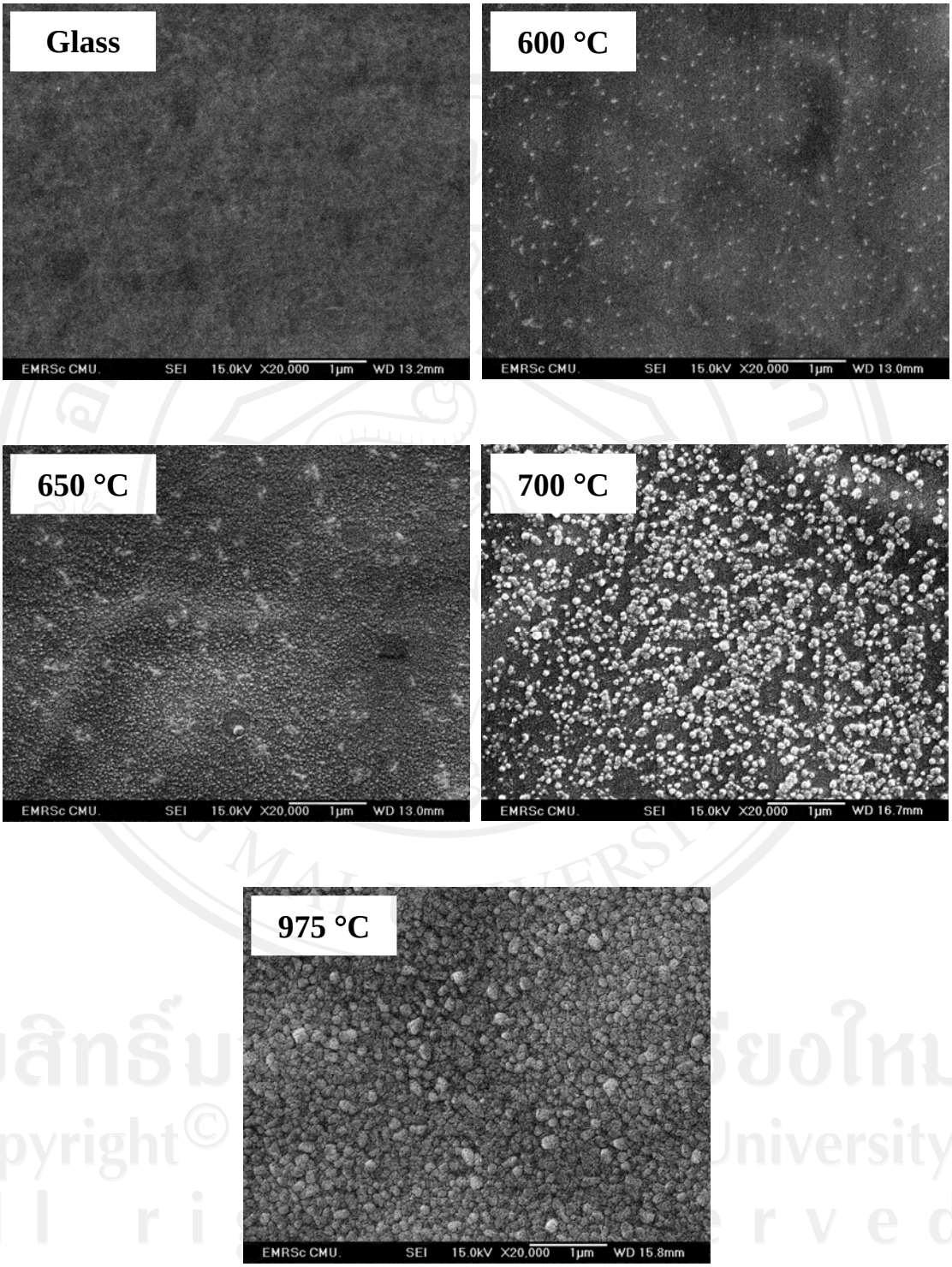

Fig. 4.23 SEM micrographs of the glass and glass-ceramic samples with 35 mol% SiO_2.

In principle, phase separation in glass forming melts is a well-known phenomenon. It might occur above the liquidus temperature, for example in the $MgO \cdot SiO_2$, $CaO \cdot SiO_2$ and $PbO \cdot SiO_2$ [95] systems. A liquid of a composition within such a miscibility gap, during cooling usually shows phase separation and subsequent sedimentation and finally two glassy layers with different compositions. Systems exhibiting metastable liquid-liquid phase separation (below the liquidus temperature), such as the systems $BaO \cdot SiO_2$ [96] or $Na_2O \cdot B_2O_3 \cdot SiO_2$ [97] widely enable to tailor the microstructure, for example the sizes of droplets or interpenetrating structures by heat treatment. Here, the phase separation process is much slower, because of the higher viscosities of the respective liquids. These effects have been intensively studied since the pioneer investigations of Porai-Koshits [98] and Vogel [99]. A phase-separated droplet structure is a good prerequisite for a subsequent crystallization process. In many cases, the crystal formed from the droplet phase has a size comparable to that of the droplet.

This facilitates the tailoring of the final size of the crystallites. For example in the case of apatite glass-ceramics [100], droplets enriched in CaO and P_2O_5 which are formed during heating are transferred to crystalline apatite. In the present case, however, the droplet phase, which is enriched in silica, does not crystallize during heating. However, the matrix phase is crystallized and forms lithium niobate. This leads to a microstructure which is composed of a continuous ferroelectric phase with embedded SiO_2 droplets and is supposed to possess favorable dielectric properties. Usually, a droplet structure is considered as a binodal structure, while an interpenetrating microstructure is supposed as spinodal. It should, however, be mentioned that the structure may change during the course of the cooling process and

hence, the attribution of a certain structure to binodal or spinodal is never completely clear. In our case, the structures in the case of ≥ 40 mol% SiO_2 is that of droplets and hence supposedly bimodal (Fig. 4.17 - Fig. 4.18), while 35 mol% SiO_2, the structure might be interpenetrating and hence probably spinodal (Fig. 4.16). The miscibility gap hence seems to process a maximum near 35 mol% SiO_2. At smaller SiO_2 content again a droplet structure is formed.

It should be noted that in all previous studies on the $LiNbO_3 \cdot SiO_2$ system, the SiO_2 content was much larger than in the present study, using the incorporation method.

4.6 Optical properties

4.6.1. Transmittance (%)

The optical transmission spectra of $(100\text{-}x)LiNbO_3 \cdot xSiO_2$ (with x = 25, 30 and 35) glasses and glass-ceramics were all recorded at room temperature as shown in Fig. 4.24 - Fig. 4.26. The glass samples are optically transparent. By analogy, glass-ceramic samples were heat-treated at 580 and 600 °C to be transparent samples. However, the glass-ceramic samples heat-treated at 625 °C show slightly smaller transmittance in the UV-Vis-NIR spectra and the images show slight light scattering due to the slightly large crystallite sizes of the $LiNbO_3$. The transmittance lines of glass-ceramic samples heat-treated at 650 °C are close to 0% as their appearances are translucent. The glass-ceramics heat-treated at 700 and 975 °C, were opaque due to the occurrence of larges crystals. For visible light (wavelength 400 to 800 nm), samples containing crystals larger than 200 nm should show light scattering and hence the respective samples should be opaque [91]. Transparent samples should possess crystals less than 200 nm and also have a small crystal size distribution.

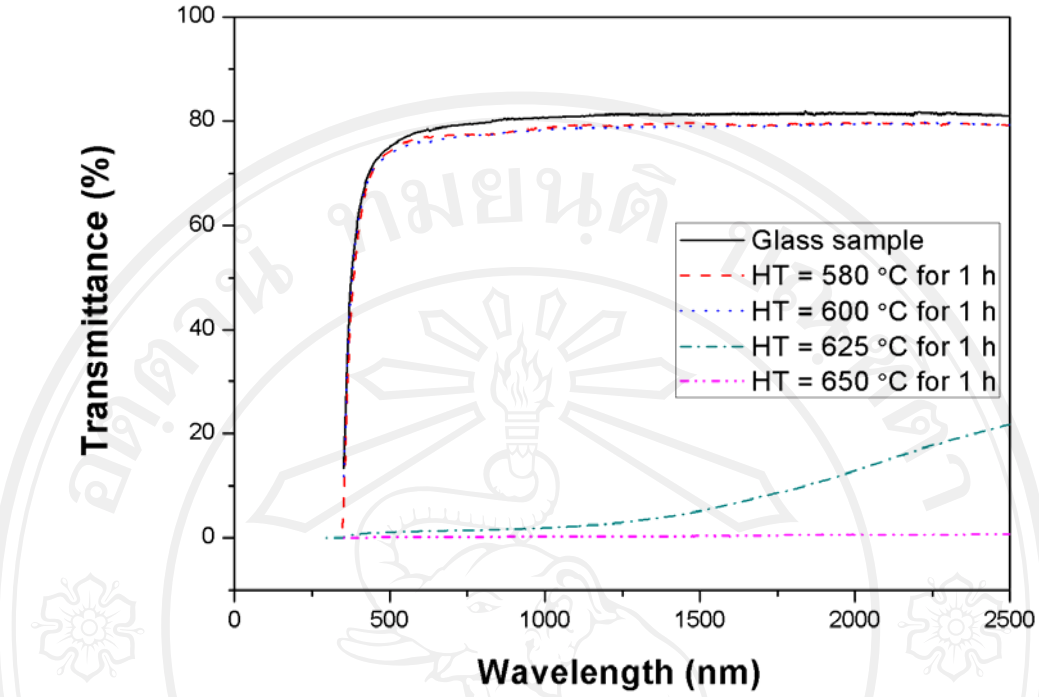

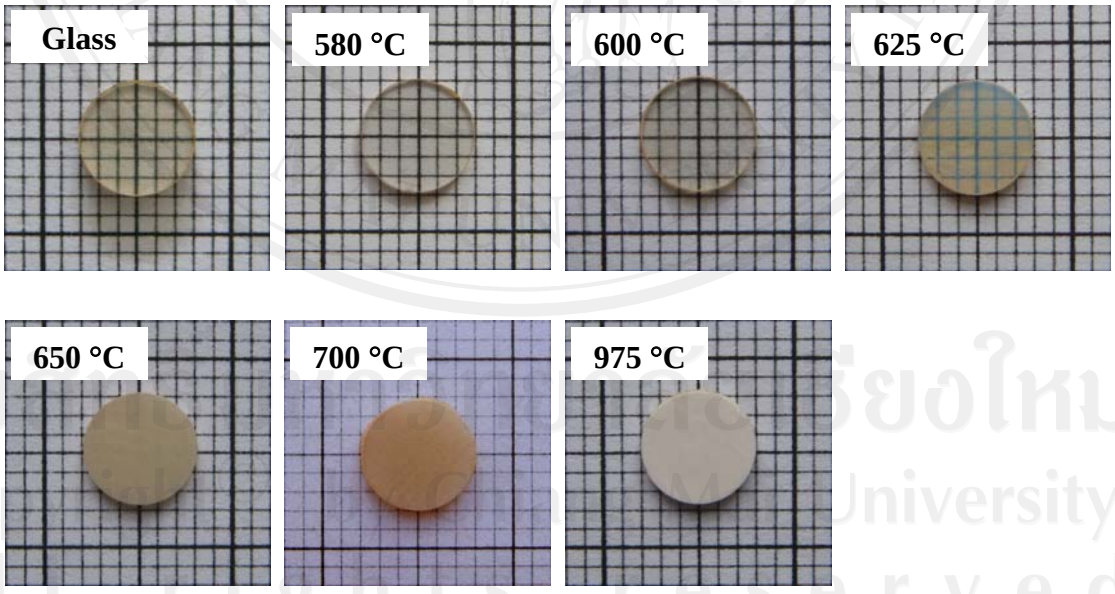

Fig. 4.24 The optical transmission spectra and images of glass and glass-ceramic samples with 25 mol% SiO_2 (minor scale = 1 mm).

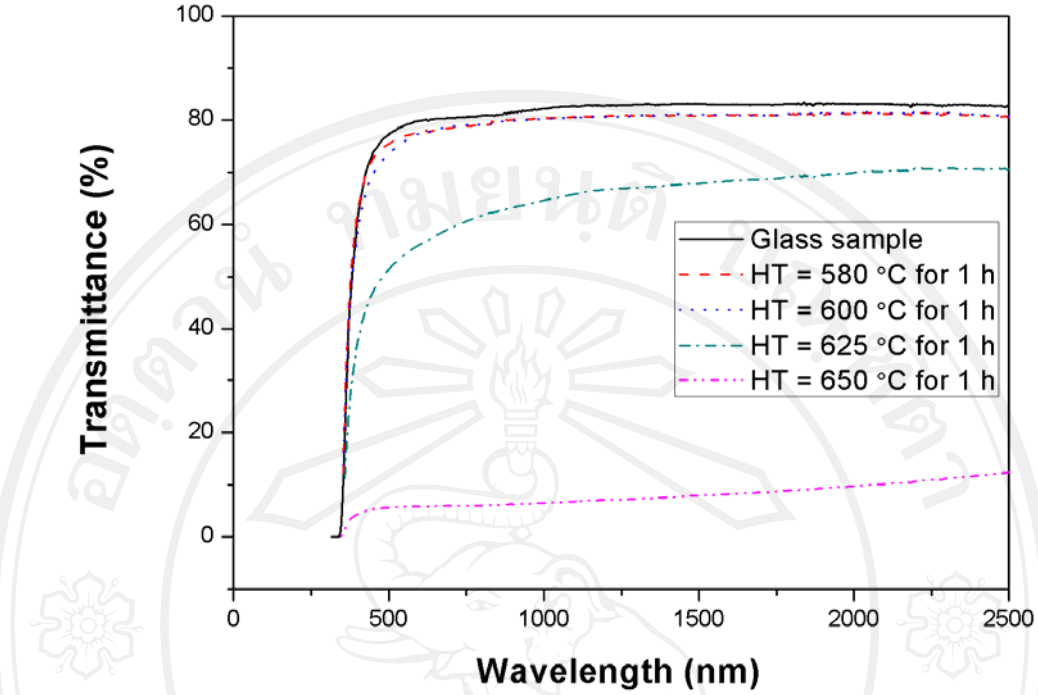

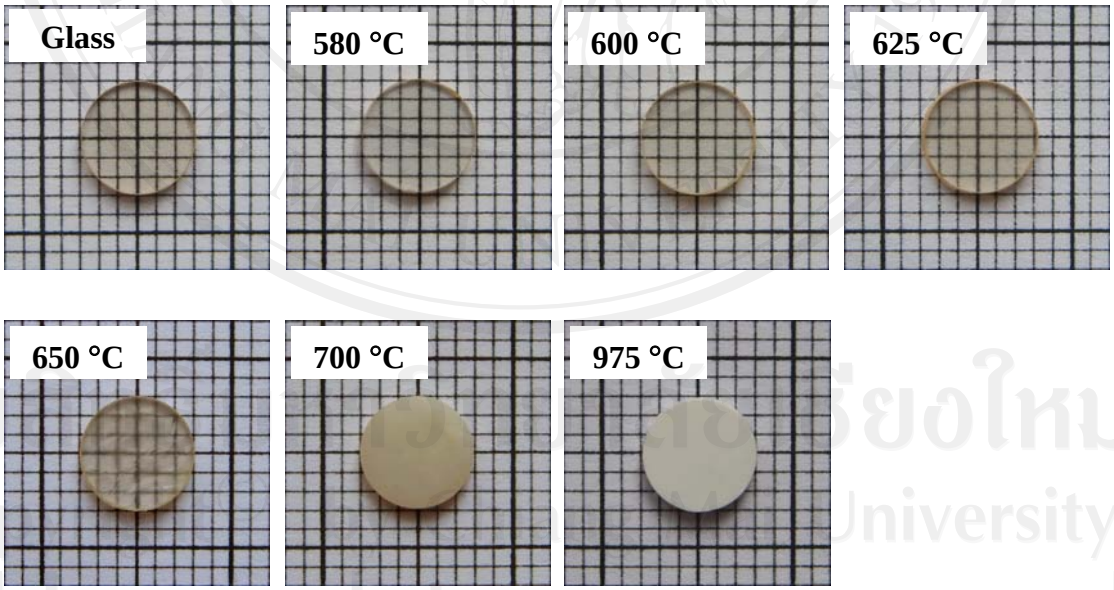

Fig. 4.25 The optical transmission spectra and images of glass and glass-ceramic samples with 30 mol% SiO_2 (minor scale = 1 mm).

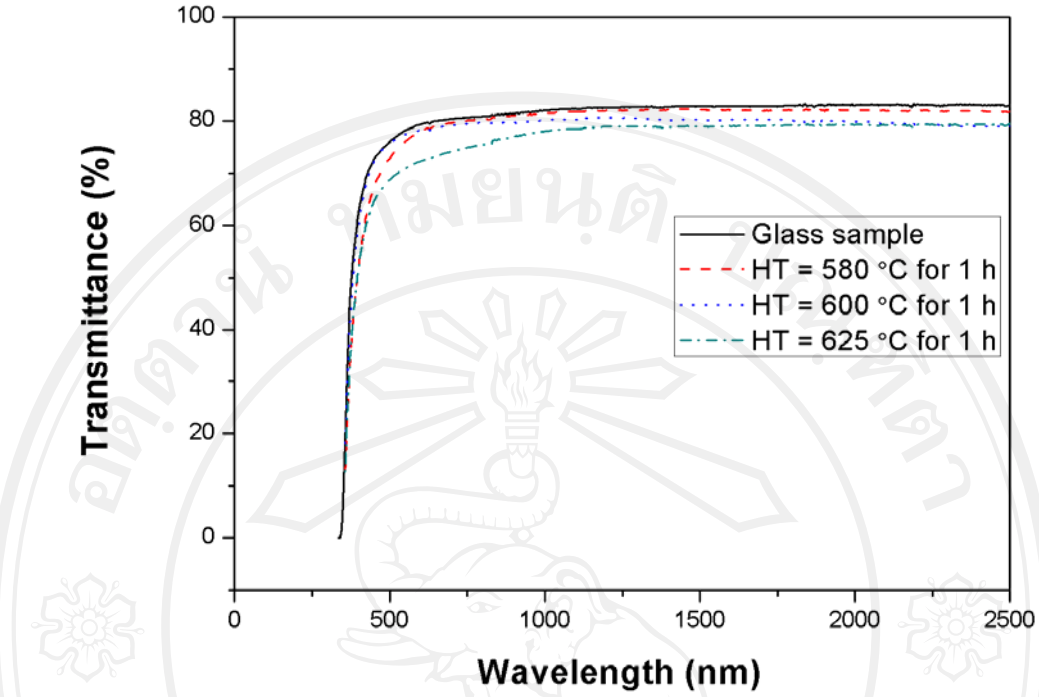

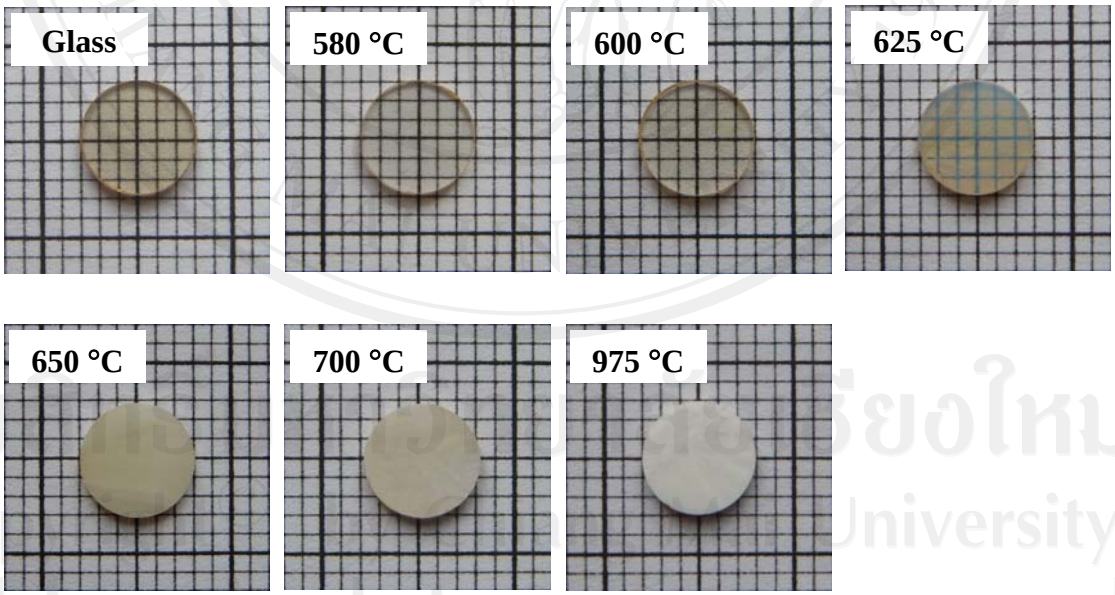

Fig. 4.26 The optical transmission spectra and images of glass and glass-ceramic samples with 35 mol% SiO_2 (minor scale = 1 mm).

4.6.2 Refractive index

The refractive indices (n) of the (100-x)$LiNbO_3$ · $xSiO_2$ (with x = 20, 40, 50 and 60) glass samples were predicted and calculated by SciGlass 6.6 which are 2.003, 1.882, 1.823 and 1.763, respectively as shown in Fig. 4.27. The SiO_2 content increased with decreasing refractive index. This may be caused by the smaller value of the refractive index of SiO_2 (n = 1.455) than that of the $LiNbO_3$ (n = 2.283).

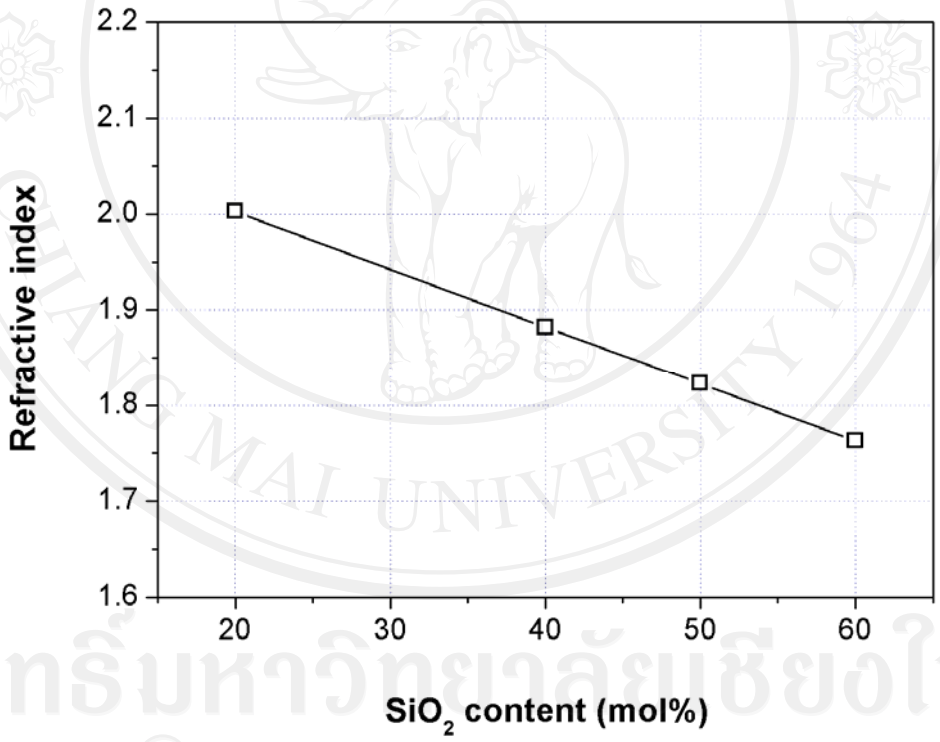

Fig. 4.27 Refractive index of glass samples.

4.7 Electrical property

The electrical property of the (100-*x*)$LiNbO_3 \cdot xSiO_2$ (with x = 25, 30 and 35) glasses and glass-ceramics were measured in terms of capacitance (C). Then, it was converted to relative permittivity (ε_r).

The variation of relative permittivity (ε_r) as a function of frequency (f) for the samples with x = 25 is shown in Fig. 4.28 and Table 4.5 for various temperatures. The ε_r values of the glass-ceramic samples heat-treated at 600, 650, 700 and 975 °C for 1 h were larger than that of the glass samples. Moreover, it was found to increase with increasing heat treatment temperature, however, with increasing frequency, the ε_r values decreased. For the ε_r values of the sample with x = 30 (Fig. 4.29 and Table 4.6), the dielectric loss (tan δ) values at 100 kHz are 0.12 and 0.063 after heat-treated at 600 and 700 °C for 1 h, respectively and 35 (Fig. 4.30 and Table 4.7), the tendency was the same to that of the sample with x = 25, but only the ε_r values of the 25 mol% SiO_2 sample were much more than that of 30 and 35 mol% SiO_2 samples (25 mol% SiO_2 > 30 mol% SiO_2 > 55 mol% SiO_2). Fig. 4.31 shows the frequency dependence of ε_r for 20 - 35 mol% SiO_2 glass-ceramic samples heat-treated at 700 °C for 1 h. It can be clearly seen that the more the SiO_2 content is in the glass-ceramic samples, the lower the ε_r value becomes.

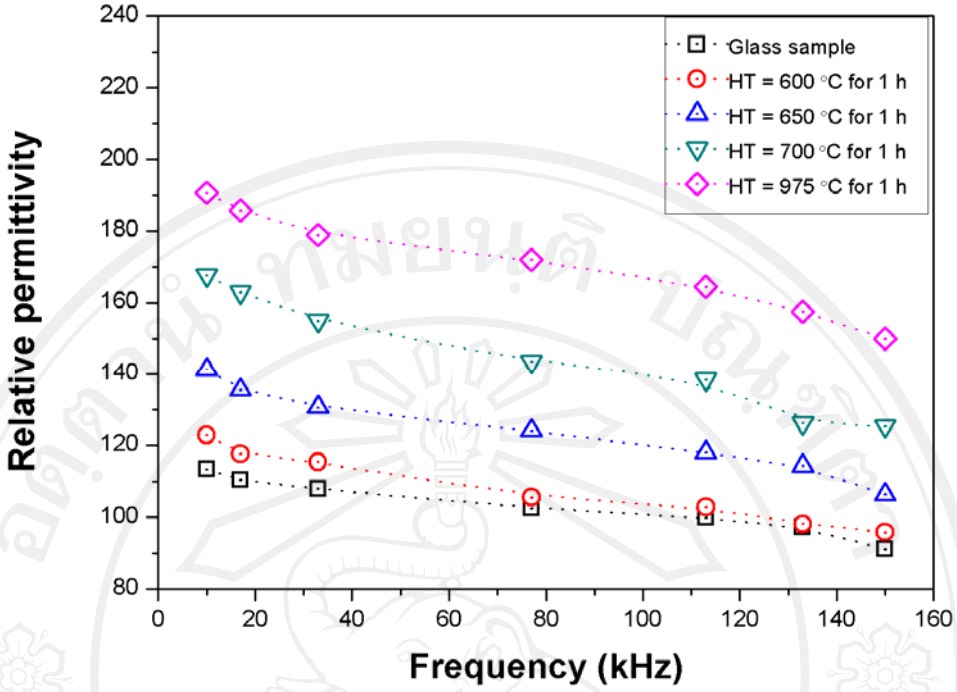

Fig. 4.28 Variation of relative permittivity (ε_r) as a function of frequency with 25 mol% SiO_2.

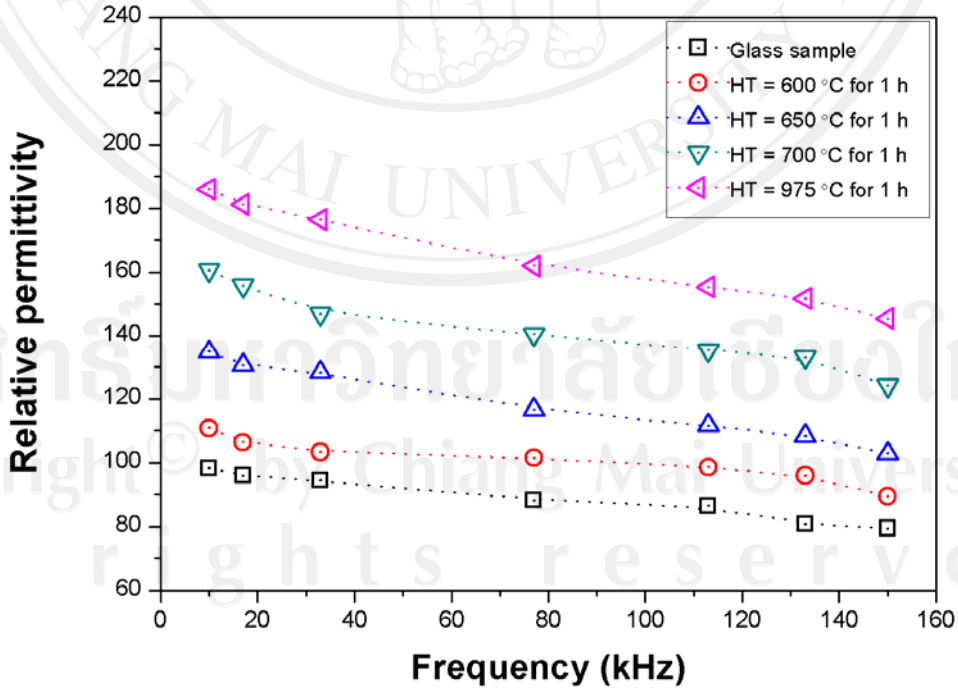

Fig. 4.29 Variation of relative permittivity (ε_r) as a function of frequency with 30 mol% SiO_2.

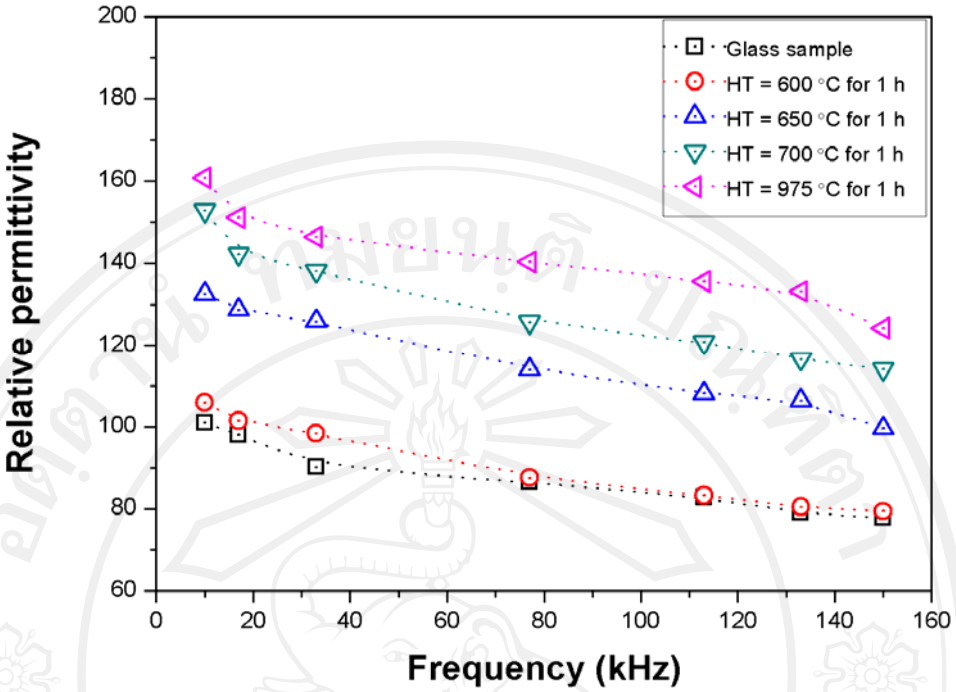

Fig. 4.30 Variation of relative permittivity (ε_r) as a function of frequency with 35 mol% SiO_2.

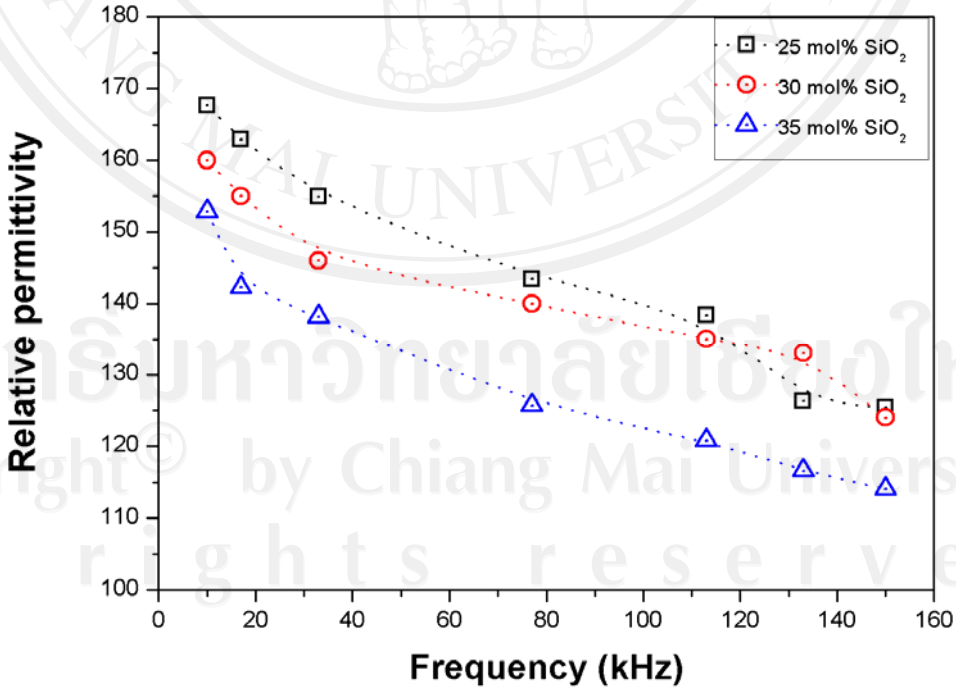

Fig. 4.31 Relative permittivity (ε_r) of glass and glass-ceramic samples with 25, 30 and 35 mol% SiO_2 as heat-treated at 700 °C for 1 h.

Table 4.5 Relative permittivity (ε_r) of glass and glass-ceramic samples at 600, 650, 700 and 975 °C for 1 h with 25 mol% SiO_2.

Frequency (kHz)	Relative permittivity (ε_r)				
	Glass samples	**HT = 600 °C**	**HT = 650 °C**	**HT = 700 °C**	**HT = 975 °C**
10	113.34	122.86	141.23	167.65	190.67
17	110.25	117.66	135.47	162.87	185.84
33	107.87	115.42	130.64	154.90	178.91
77	102.51	105.54	124.08	143.46	171.97
113	99.80	102.79	117.99	138.38	164.42
133	97.25	98.06	114.24	126.27	157.53
150	91.11	95.78	106.31	125.36	150.01

Table 4.6 Relative permittivity (ε_r) of glass and glass-ceramic samples at 600, 650, 700 and 975 °C for 1 h with 30 mol% SiO_2.

Frequency (kHz)	Relative permittivity (ε_r)				
	Glass samples	**HT = 600 °C**	**HT = 650 °C**	**HT = 700 °C**	**HT = 975 °C**
10	98.12	110.80	134.81	160.53	185.99
17	95.85	106.36	130.52	155.74	181.25
33	94.40	103.27	128.22	146.79	176.47
77	88.07	101.47	116.57	140.48	161.95
113	86.41	98.55	111.59	135.35	155.36
133	80.75	95.89	108.33	133.07	151.75
150	79.38	89.42	102.76	124.18	145.39

Table 4.7 Relative permittivity (ε_r) of glass and glass-ceramic samples at 600, 650, 700 and 975 °C for 1 h with 35 mol% SiO_2.

Frequency (kHz)	Relative permittivity (ε_r)				
	Glass samples	**HT = 600 °C**	**HT = 650 °C**	**HT = 700 °C**	**HT = 975 °C**
10	100.98	105.86	132.52	152.86	160.84
17	98.07	101.46	128.65	142.27	151.16
33	90.12	98.37	125.88	138.18	146.47
77	86.55	87.58	113.97	125.68	140.33
113	82.76	83.24	108.11	120.81	135.6
133	79.04	80.5	106.34	116.59	133.19
150	77.67	79.43	99.56	114.07	124.22